Chapter 3

Phytoplankton community structure in relation to vertical stratification along a north-south gradient in the Northeast Atlantic Ocean

Kristina D. A. Mojica[1], Willem H. van de Poll[1], Michael Kehoe[2], Jef Huisman[2], Klaas R. Timmermans[1, 3], Anita G. J. Buma[3], Hans J. van der Woerd[4], Lisa Hahn-Woernle[5], Henk A. Dijkstra[5] and Corina P. D. Brussaard[1,2]

[1]Department of Biological Oceanography, NIOZ - Royal Netherlands Institute for Sea Research, NL 1790 AB, Den Burg, Texel, The Netherlands
[2]Department of Aquatic Microbiology, Institute for Biodiversity and Ecosystem Dynamics (IBED), University of Amsterdam, P.O. Box 94248, 1090 GE, Amsterdam, The Netherlands
[3]Department of Ocean Ecosystems, Energy and Sustainability Research Institute Groningen, University of Groningen, Nijenborgh 7, 9747 AG Groningen, The Netherlands
[4]Institute for Environmental Studies (IVM), VU University Amsterdam, De Boelelaan 1087, 1091 HV, Amsterdam, The Netherlands
[5]Institude for Marine and Atmospheric research Utrecht (IMAU), Department of Physics and Astronomy, Utrecht University, Princetonplein 5, 3584 CC Utrecht, The Netherlands

Limnology and Oceanography (2015) doi: 10.1002/lno.10113

Abstract

Climate change is affecting the hydrodynamics of the world's oceans. How these changes will influence the productivity, distribution and abundance of phytoplankton communities is an urgent research question. Here we provide a unique high-resolution mesoscale description of the phytoplankton community composition in relation to vertical mixing conditions and other key physicochemical parameters along a meridional section of the Northeast Atlantic Ocean. Phytoplankton, assessed by a combination of flow cytometry and pigment fingerprinting (HPLC-CHEMTAX), and physicochemical data were collected from the top 250 m water column during the spring of 2011 and summer of 2009. Multivariate analysis identified water column stratification (based on 100 m depth-integrated Brunt-Väisälä frequency N^2) as one of the key drivers for the distribution and separation of different phytoplankton taxa and size classes. Our results demonstrate that increased stratification (i) broadened the geographic range of *Prochlorococcus* as oligotrophic areas expanded northward, (ii) increased the contribution of picoeukaryotic phytoplankton to total autotrophic organic carbon (< 20 μm), and (iii) decreased the abundances of diatoms and cryptophytes. We discuss the implications of our findings for the classification of phytoplankton functional types in biogeochemical and ecological ocean models. As phytoplankton taxonomic composition and size affects productivity, biogeochemical cycling, ocean carbon storage and marine food web dynamics, the results provide essential information for models aimed at predicting future states of the ocean.

Introduction

The oceans play an essential role in regulating global climate through the storage and transportation of heat and the uptake and sequestration of carbon dioxide (Levitus et al. 2000; Hoegh-Guldberg and Bruno 2010). As global warming continues, the surface waters of the ocean are envisaged to rise by 2-6°C over the next 100 years (Meehl et al. 2007; Collins et al. 2013). Ocean-climate models predict that surface warming, in combination with changes in freshwater input at high latitudes (due to rises in precipitation, land run off and sea ice melt) will lead to increases in vertical stratification (Sarmiento et al. 1998; Sarmiento 2004). Vertical stratification affects the production of the world's oceans as it determines the general availability of light and nutrients to phytoplankton in the ocean (Behrenfeld et al. 2006; Huisman et al. 2006; Hoegh-Guldberg and Bruno 2010). Stratification suppresses turbulence and reduces the mixed layer depth, thereby relaxing light limitation but at the same time restricting the flow of nutrients from depth (Mahadevan et al. 2012). In temperate and high latitude regions, the annual establishment of seasonal stratification often triggers the highly productive phytoplankton spring bloom (Sverdrup 1953; Huisman et al. 1999; Siegel et al. 2002). However, strong and prolonged stratification often leads to ocean oligotrophication as phytoplankton become nutrient limited by depletion of the nutrients in the surface layer. As a consequence of increases in sea surface temperature (SST) and resultant increases in vertical stratification, oligotrophic areas (i.e., defined as areas below 0.07 mg Chl m^{-3}) of the North Atlantic subtropical gyre are estimated to be expanding at a rate of up to 4.3% yr^{-1} (Polovina et al. 2008).

Projected alterations to stratification and vertical mixing have the potential to affect phytoplankton species composition (Huisman et al. 2004), phenology (Edwards and Richardson 2004), productivity (Gregg et al. 2003; Behrenfeld et al. 2006; Polovina et al. 2008), size structure (Li 2002; Daufresne et al. 2009; Hilligsøe et al. 2011), nutritional value (Mitra and Flynn 2005; van de Waal et al. 2010), abundance (Richardson and Schoeman 2004) and spatial distribution (Doney et al. 2012; van de Poll et al. 2013). Consequently, affecting the functioning and biogeochemistry of pelagic and benthic ecosystems, and altering their capacity for carbon sequestration (Beaugrand 2009; Hoegh-Guldberg and Bruno 2010). Understanding the ecological and physiological mechanisms controlling changes in phytoplankton community structure across gradients of vertical stability is therefore vital to assessing the response of marine systems to global climate change.

The North Atlantic Ocean is key to global climate and ocean circulation, due to North Atlantic deep water formation, accounting for 20% of the net ocean uptake of CO_2 (Deser and Blackmon 1993; Dawson and Spannagle 2008). The Northeast Atlantic Ocean provides a meridional gradient in stratification, with permanent stratification in the subtropics and seasonal stratification in the temperate zones (Talley et al. 2011; Jurado et al. 2012a). To assess potential alterations in phytoplankton community structure of the North Atlantic due to future changes in vertical stratification, a firm baseline is required that accurately describes the status quo. Yet, even for the relatively well-investigated North Atlantic, comprehensive descriptions of phytoplankton community structure in relation to vertical stratification patterns at the ocean basin scale are scarce (Partensky et al. 1996; Tarran et al. 2006; Bouman et al. 2011). Here we investigate how phytoplankton abundance, size and community composition are related to vertical stratification along a latitudinal gradient in the Northeast Atlantic Ocean during spring and summer. Comparison between two seasons with different vertical density distributions offers an unique opportunity to study how phytoplankton dynamics change as stratification develops. The results presented here provide an important baseline to study the effect of future climate change on marine ecosystems in the North Atlantic.

Methods

Study area and sampling procedure

During two research cruises, STRATIPHYT I taking place in the summer (July-August) of 2009 and STRATIPHYT II in spring (April-May) of 2011, samples were collected over a transect traversing a North-South stratification gradient in the Northeast Atlantic Ocean (Fig. 1) on board of the R/V Pelagia. During each cruise, thirty-two stations (separated by approximately 100 km) were sampled over the course of a month in the area located between 29°N and 63°N, which spans from the Canary Islands to Iceland. Water samples were collected in the top 250 m from at least 10 separate depths using 24 plastic samplers (General Oceanics type Go-Flow, 10 liter) during STRATIPHYT I and Teflon samplers (NIOZ design Pristine Bottles, 27 liters) during STRATIPHYT II. Samplers were mounted on an ultra-clean (trace-metal free) system consisting of a fully titanium sampler frame equipped with CTD (Seabird 9+; standard conductivity, temperature and pressure sensors) and auxiliary sensors for chlorophyll autofluorescence (Chelsea

Aquatracka Mk III), light transmission (Wet-Labs C-star) and photosynthetic active radiation (PAR; Satlantic). Data from the chlorophyll autofluorescence sensor were calibrated against HPLC data according to van de Poll et al. (2013) in order to determine total Chlorophyll *a* (Chl *a*) for the present study. Samples were taken inside a 6 m Clean Container from each depth for inorganic nutrients (5 ml), flow cytometry (10 ml), and phytoplankton pigments (10 L).

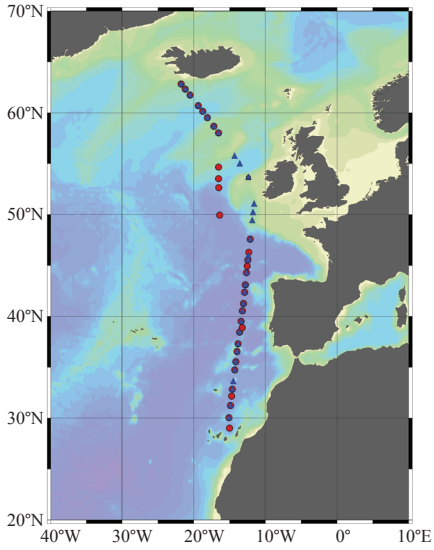

Figure 1. Ocean Data View (ODV) (Schlitzer, 2002) bathymetric map of the Northeast Atlantic Ocean depicting station locations for the summer 2009 (blue triangles) and spring 2011 (red circles) STRATIPHYT cruises.

Physicochemical data

Temperature eddy diffusivity (K_T) data, referred to here as the vertical mixing coefficient, were derived from temperature and conductivity microstructure profiles measured using the commercial microstructure profiler SCAMP (Self Contained Autonomous Microprofiler) (Stevens et al. 1999). A detailed description of SCAMP methodology and data for both STRATIPHYT cruises have been described by Jurado et al. (2012 a,b). The SCAMP was deployed at fewer stations (i.e., 17 and 14 in spring and summer, respectively) and to lower depths (up to 100 m) than the remainder of the data (23 stations and up to 250 m depth) in the present study. In order to correct for this deficiency, data were interpolated using the spatial kriging function 'krig' executed in R using the 'fields' package (Furrer et al. 2012).

Interpolated K_T values were bounded below by the minimum value measured for each of the two cruise datasets; the upper values were left unbounded. This resulted in estimated K_T values which preserved the qualitative pattern and range of values previously reported (Jurado et al. 2012a; Jurado et al. 2012b), i.e., continuous stratification during the summer STRATIPHYT I cruise and two distinct zones of mixing during the spring STRATIPHYT II cruise; stratification in the south and deep strong mixing in the north. SCAMP data were also used to quantify the strength of background stratification according to the square of the Brunt-Väisälä frequency: $N^2 = (g/\rho)(\partial\rho/\partial z)$ where z is depth measured positively downward (m), ρ is the density of water (kg m^{-3}) and g is the gravitational acceleration (9.8 m s^{-2}) (Houry et al. 1987; Jurado et al. 2012a; Jurado et al. 2012b). The Brunt-Väisälä frequency represents the angular velocity (i.e., the rate) at which a small perturbation of the stratification will re-equilibrate. Hence, it is a simple measure of the stability of the vertical stratification. N^2 values were depth averaged over the top 100 m of the water column and classified based on the following criteria: $N^2 < 2x10^{-5}$ rad^2 s^{-2} for non-stratified, $2x10^{-5} < N^2 < 5x10^{-5}$ rad^2 s^{-2} for weakly stratified and $N^2 > 5x10^{-5}$ rad^2 s^{-2} for strongly stratified. In addition, the depth of the mixed layer (Z_m), was determined as the depth at which the temperature difference with respect to the surface was 0.5°C (Levitus et al. 2000; Jurado et al. 2012b). As shown by Brainerd and Gregg (1995), this definition of the mixed layer provides an estimate of the depth through which surface waters have been mixed in recent days. On the few occasions where SCAMP data were not available Z_m was determined from CTD data. Station mean temperature profiles obtained from SCAMP and CTD measurements were compared and were found to have a good correlation.

Discrete water samples for dissolved inorganic phosphate (PO_4^{3-}), ammonium (NH_4^+), nitrate (NO_3^-), and nitrite (NO_2^-) were gently filtered through 0.2 µm pore size polysulfone Acrodisk filters (32 mm, Pall Inc.), after which samples were stored at -20°C until analysis. Dissolved inorganic nutrients were analyzed onboard using a Bran+Luebbe Quaatro AutoAnalyzer for dissolved orthophosphate (Murphy and Riley 1962), inorganic nitrogen (nitrate + nitrite: NO_x) (Grasshoff 1983) and ammonium (Koroleff 1969; Helder and De Vries 1979). Detection limits ranged between the two cruises from 0.06-0.10 µM for NO_x, 0.010-0.028 µM for PO_4^{3-} and 0.05-0.09 µM for NH_4^+.

Phytoplankton data

Phytoplankton consisting of photoautotrophic prokaryotic cyanobacteria and eukaryotic algae < 20 µm were enumerated on fresh samples using a Becton-Dickinson FACSCalibur flow cytometer (FCM) equipped with an air-cooled Argon laser with an excitation wavelength of 488 nm (15 mW). Samples were measured for 10 minutes using a high flow rate with the discriminator set on red chlorophyll autofluorescence. Phytoplankton populations were distinguished using bivariate scatter plots of autofluorescent properties (orange autofluorescence from phycoerythrin for the cyanobacteria *Synechococcus* spp. and red autofluorescence from Chl *a* for photoautotrophs) against side scatter. The obtained list-mode files were analyzed using the freeware CYTOWIN (Vaulot 1989).

Regularly throughout the cruise transect, size-fractionation was performed to provide average cell size for the different phytoplankton subpopulations. Specifically, a whole water sample (10 ml) was size-fractionated by sequential gravity filtration through 8, 5, 3, 2, 1, 0.8, and 0.4 μm pore-size polycarbonate filters. Each fraction was then analyzed using FCM as described above. The equivalent spherical diameter for each population was determined as the size displayed by the median (50%) number of cells retained for that cluster. In total 9 different phytoplankton populations were distinguished, consisting of 6 eukaryotic and 3 cyanobacterial populations, i.e., *Synechococcus* spp. (average size range between the two cruises of 0.9-1.0 µm), *Prochlorococcus* high light population (HL; 0.6 µm) and *Prochlorococcus* low light population (LL; 0.7-0.8 µm). The photosynthetic eukaryotic populations consisted of 2 pico-sized groups, i.e., Pico I (1.0-1.4 µm) and Pico II (1.5-2.0 µm), and 4 nano-sized groups, i.e., Nano I (3-4 µm), Nano II (6-8 µm), Nano III (8-9 µm) and Nano IV (9 µm). In order to estimate the contribution of the different phytoplankton groups to carbon biomass, carbon-conversion factors were applied to FCM cell counts. Specifically, cell counts were transformed assuming spherical diameters equivalent to the average cell size determined from size fractionation and applying conversion factors of 237 fg C μm^{-3} (Worden et al. 2004) and 196.5 fg C μm^{-3} for pico- and nano-sized plankton (Garrison et al. 2000), respectively.

Phytoplankton taxonomic composition was determined by pigment analysis of 10 L GF/F filtered samples (47 mm, Whatman; flash frozen and stored at -80°C until analysis) using HPLC as described by Hooker et al. (2009). In short, filters were freeze-dried (48 h) and pigments extracted using 5 ml 90% acetone (v/v, 48 h, 4°C, darkness) and separated using a HPLC (Waters 2695 separation module, 996 photodiode array detector) equipped with a Zorbax Eclipse XDB-C_8 3.5 µm column

(Agilent Technologies, Inc.). Peak identification was based on retention time and diode array spectroscopy. Pigments standards (DHI LAB products) were used for quantification of chlorophyll a_1, chlorophyll a_2, chlorophyll *b*, chlorophyll c_2, chlorophyll c_3, peridinin, 19-butanoyloxyfucoxanthin, 19-hexanoyloxyfucoxanthin, fucoxanthin, neoxanthin, prasinoxanthin, alloxanthin, and zeaxanthin. The sum of chlorophyll *a* and divinyl chlorophyll *a* was used as indicator for algal biomass as these pigments are universal in algae and *Prochlorococcus*. Specific marker pigments were used to reveal the presence of taxonomically distinct pigment signatures using CHEMTAX (version 195; Mackey et al. 1996) software, thereby estimating the concentration of each taxonomic group relative to chlorophyll *a*. CHEMTAX was run separately for oligotrophic and non-oligotrophic stations and for spring and summer samples. Oligotrophic areas defined by nutrient (i.e., $NO_3^- \leq 0.13$ µM and $PO_4^{3-} \leq 0.03$ µM; van de Poll et al. 2013) or by Chl *a* concentrations (< 0.07 mg Chl m^{-3}), delineating regions south of 40°N and 45°N as oligotrophic for the spring and summer, respectively. CHEMTAX was run with 500 iterations, with all elements varied (100% for chlorophyll *a* and divinyl chlorophyll *a* and 500% for the other pigments). Initial pigment ratios in the iterations were based on van de Poll et al. (2013), where high-light initial pigment ratios were implemented for surface samples (0-50 m) of oligotrophic stations and low-light initial pigment ratios for subsurface samples (> 50 m) of oligotrophic and all non-oligotrophic samples. In order to compare to taxonomic composition data provided by CHEMTAX, the percent contribution of different FCM distinguished groups to total carbon biomass (< 20 µm) was also determined. Likewise, Chl *a* and CHEMTAX taxonomic composition were used to determine the group-specific Chl *a* concentrations.

In order to provide additional taxonomic information, seawater samples were also fixed for occasional microscopic analysis. Specifically, 150 ml of seawater was fixed in Lugol's iodine solution (1% final concentration) supplemented with formaldehyde and stored at 4 °C until analysis. Samples were processed according to the Utermöhl method (Edler and Elbrächter 2010). Briefly, 10-50 ml of fixed sample was aliquoted into a settling chamber and after a 48 h settling time, phytoplankton species composition was determined along one or two meridians at 40x and 200x magnification using an Olympus IMT-2 inverted microscope.

Statistical Analysis

Measured quantities included in the multivariate analysis were: the vertical mixing coefficient, N^2, temperature, salinity, density, PO_4^{3-}, NH_4^+, NO_2^- and NO_3^-. The ratio

of nitrogen to phosphorus (N:P) was also included and calculated as the ratio of total dissolved inorganic nitrogen (i.e., NO_2^- + NO_3^- + NH_4^+) to PO_4^{3-}. In addition, several variables were included as factors (i.e., single value per station/sample) in order to better discriminate how environmental conditions relate to phytoplankton abundance and taxonomic composition. These included depth layer, euphotic depth, stratification level, mixed layer depth, the ratio of mixed layer depth to the euphotic depth and nutrient flux of NO_3^-, NO_2^- and PO_4^{3-} into both the mixed layer and euphotic zone. The depth of each sample was classified as either within the mixed layer (Z_m) or below mixed layer depth (BZ_m). Euphotic depth (Z_{eu}), calculated based on the light attenuation coefficient (K_d), was defined as the depth at which irradiance was 0.1% of the surface value (Moore and Chisholm 1999) in order to account for the dominance and vertical distribution (down to 200 m) of *Prochlorococcus*. The ratio of the mixed layer depth to the euphotic depth (Z_m/Z_{eu}) was used as an index of light availability in the mixed layer. Thus, if mixed layer depth exceeds the euphotic depth (i.e., $Z_m/Z_{eu} > 1.0$), phytoplankton cells are more likely to be exposed to light limited conditions. Finally, the nutrient flux at a depth z* was defined as $\varphi(z^*)=-K_T(z)(\partial N/\partial z)|_{z^*}$ and calculated based on measured vertical profiles of the vertical mixing coefficient (K_T) and individual nutrients (N) of PO_4^{3-}, NO_2^- and NO_3^-. The nutrient fluxes were determined at the depths Z_{eu} and Z_m, and coded according to the depth and nutrient being considered, e.g. $Z_{eu}PO_4$ represents the PO_4^{3-} flux into the euphotic zone.

A multivariate statistical analysis was performed using the R statistical software (R Development Core Team 2012) supplemented by vegan (Oksanen et al. 2013). Data exploration was carried out following the protocol described in Zuur et al. (2010). Because CHEMTAX pigment data and FCM abundance data occasionally did not coincide, each dataset was analyzed separately in order to maximize the size of the data matrices. In addition, depth profiles of N^2 were restricted to depths less than 100 m due to the limitations of the SCAMP. Consequently, N^2 was incorporated into the analysis as the factor stratification level according to Fig. 2. FCM phytoplankton carbon (C) data, N:P, NH_4^+, and all nutrient fluxes were log (x+1) transformed and vertical mixing coefficient and Z_m/Z_{eu} were log transformed in order to reduce the effect of outliers. In order to identify and remove collinearity, variance inflation factors (VIF) were calculated using the R function corvif written by Zuur et al. (2009). Sequentially, explanatory variables with the largest VIF were removed until all variables resulting in VIF < 10. Two exceptions were the removal of NO_3^- instead of PO_4^{3-} (Pearson correlation: $r = 0.99$, $p < 0.001$) and the

removal of $Z_{eu}NO_2$ instead of $Z_{eu}PO_4$ (Pearson correlation: r = 0.96; $p < 0.001$). Any residual collinearity was identified and removed based on correlation pair plots and boxplots of variables across factor levels. At this stage, the vertical mixing coefficient was excluded due to collinearity with stratification level and depth layer. The final selection resulted in 12 explanatory variables: Salinity, PO_4^{3-}, NH_4^+, NO_2^-, Z_{eu}, Z_m/Z_{eu}, N:P, $Z_{eu}PO_4$, Z_mPO_4, Z_mNO_2, stratification level and depth level. Initial scatter plots of response variables and covariates did not show a strong non-linear pattern and therefore redundancy analysis (RDA) (Legendre and Legendre 1998) was chosen over canonical correspondence analysis (CCA) to model the response of phytoplankton carbon data (i.e., FCM phytoplankton size fractionated C) and taxonomic community composition as a function of selected explanatory variables. In all cases, RDA was performed on a correlation matrix (i.e., all phytoplankton groups equally important) and used species conditional scaling in order to better determine the relationship between phytoplankton variables and environmental covariates. Subsequent to RDA, a forward selection procedure was applied to select only those explanatory variables that contributed significantly to the RDA model, while removing non-significant terms. Significance was assessed by a permutation test, using the multivariate pseudo-F-value as the test statistic (Zuur et al. 2009). A total of 9999 permutations were used to estimate *p*-values associated with the pseudo-F statistic. Variance partitioning was applied to the final RDA model to estimate how much of the variation in the data was explained by stratification and how much by other factors.

More specifically, multivariate analysis of phytoplankton C biomass (from FCM counts) was performed on 8 different phytoplankton groups in a total of 315 samples from various depths within the upper 200 m of 23 stations along the cruise track (i.e., 166 and 149 samples in summer and spring, respectively). Forward selection and permutation tests revealed that 9 of the 12 explanatory variables significantly ($\alpha < 0.05$) contributed to the model (Table 1). Consequently, NO_2^-, $Z_m/Z_{eu,}$ and Z_mNO_2 (pseudo-F = 1.7, 1.6 and 1.7; $p = 0.13$, 0.16 and 0.13, respectively) were removed. When phytoplankton C biomass data were expressed as group-specific percentage of total C forward selection and step-wise permutation tests showed that all 12 of the explanatory variables now significantly ($\alpha < 0.05$) contributed to the model (Table 1).

Analysis of the CHEMTAX pigment data was based on 8 different taxonomic groups and total Chl *a* from 188 samples obtained from various depths within the upper 200 m water column of 23 stations (i.e., 93 and 95 samples in summer and

spring, respectively). Forward selection and step-wise permutation tests revealed that 10 of the 12 selected variables significantly contributed to the RDA model (Table 1). Subsequently, Z_mPO_4 and Z_mNO_2 (pseudo-F = 2.4, and 1.8; p = 0.06 and 0.13, respectively) were removed. When expressed as group-specific percentage of total Chl *a*, 8 variables significantly contributed to the RDA model (Table 1). Initial analysis resulted in the removal of $Z_{eu}PO_4$ and Z_mNO_2 (pseudo-F = 2.1 and 1.6; p = 0.06 and 0.13, respectively) and subsequent analysis resulted in the further removal of N:P and Z_mPO_4 (pseudo-F = 2.2 and 1.7; p = 0.05 and 0.13, respectively). When interpreting RDA correlation triplots, line lengths of the arrows representing the covariates signify their correlation with the axis (RDA1 horizontal axis and RDA2 vertical axis). For response variables, line lengths represent how well they are represented within the RDA model. The correlation between response and explanatory variables, as well as between response variables or explanatory variables themselves, is reflected in the angles between lines. Wherein, a small angle between two lines represents a high positive correlation, a 90° angle represents no correlation and 180° a strong negative correlation.

Data matrices are accessible via ftp://dmgftp.nioz.nl/zko_public/dataset/00082.

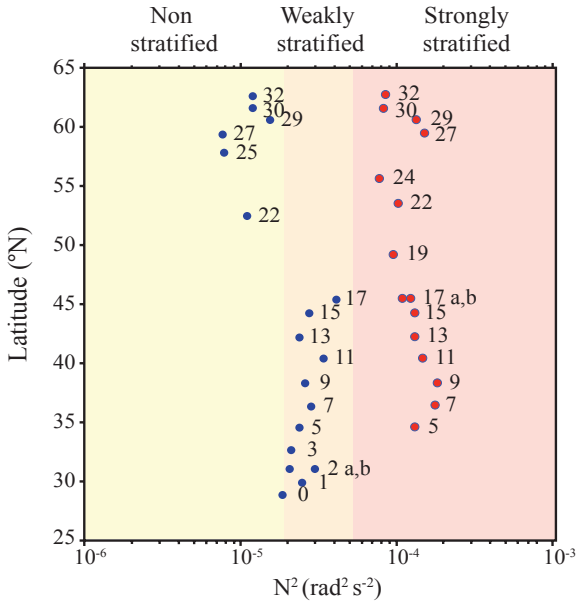

Figure 2. Brunt-Väisälä frequency (N^2) values averaged over the upper 100 m depth for the summer 2009 (red) and spring 2011 (blue) STRATIPHYT cruises and used to classification the level of stratification based on the following criteria: $N^2 < 2x10^{-5}$ rad^2 s^{-2} non-stratified, $2x10^{-5} < N^2 < 5x10^{-5}$ rad^2 s^{-2} weakly stratified and $N^2 > 5x10^{-5}$ rad^2 s^{-2} strongly stratified.

Table 1. Significance of the explanatory variables in the RDA correlation triplot of phytoplankton community composition in relation to environmental variables, as presented in Fig. 11A-D. Significance (P-value) was assessed by a permutation test, using the multivariate pseudo-F (F) as test statistic and on the Akaike Information Criterion (AIC) in case of ties (Legendre and Legendre, 1998).

A. Phytoplankton carbon			
Variable	AIC	F	P
PO_4^{3-}[a]	613.4	47.6	0.0001
Salinity[b]	551.5	70.2	0.0001
Strat. Level	511.7	23.2	0.0001
Depth Layer	500.4	13.3	0.0001
N:P	492.9	9.4	0.0001
Z_{eu}	486.7	8.1	0.0001
$Z_{eu}PO_4$	482.7	5.9	0.0002
NH_4^+	478.0	6.6	0.0002
Z_mPO_4	475.5	4.4	0.0023
B. Percentual distribution of phytoplankton carbon			
Salinity[b]	610.4	48.7	0.0001
Strat Level	582.5	16.6	0.0001
Z_{eu}	568.0	16.7	0.0001
Depth Level	544.6	15.4	0.0001
NO_2^-	549.7	6.8	0.0001
Z_mNO_2	544.8	6.8	0.0001
Z_m/Z_{eu}	541.9	4.8	0.0001
NH_4^+	539.1	4.7	0.0001
PO_4^{3-}[a]	537.4	3.6	0.0020
N:P	534.3	5.0	0.0001
$Z_{eu}PO_4$	533.9	2.2	0.0396
Z_mPO_4	533.6	2.3	0.0384
C. Chl *a* concentration			
Z_m/Z_{eu}	393.5	23.7	0.0001
Z_{eu}	377.0	19.2	0.0001
PO_4^{3-}[a]	359.0	21.1	0.0001
Salinity[b]	337.0	24.7	0.0001
Strat Level	318.6	11.4	0.0001
Depth Layer	307.8	12.7	0.0001
NH_4^+	305.3	4.3	0.0078
N:P	302.6	4.5	0.0055
$Z_{eu}PO_4$	301.1	3.3	0.0237
NO_2^-	300.0	2.9	0.0380
D. Percentual distribution of Chl *a* concentration			
Salinity[b]	356.3	41.2	0.0001
Strat Level	311.0	27.6	0.0001
Depth Layer	287.6	26.5	0.0001
Z_{eu}	269.8	20.1	0.0001
NH_4^+	266.2	5.5	0.0002
NO_2^-	263.7	4.4	0.0009
PO_4^{3-}[a]	260.0	5.5	0.0002
Z_m/Z_{eu}	256.8	4.9	0.0002

[a] $PO_4^{3-} = NO_3^-$; Pearson: $r = 0.99$, $p < 0.001$

[b] Salinity ≈ Temperature; Pearson: r=0.87, $p < 0.001$

Results

Physicochemical data

During the spring, the southern half of the cruise transect (29-46°N; stations 0-17) was classified as weakly stratified with $2x10^{-5} < N^2 < 5x10^{-5}$ rad^2 s^{-2} (Fig. 2) and Z_m depths ranged from 22 to 67 m. While the northern part (53-62°N; stations 22-32) of the transect had $Z_m > 100$ m and was considered as non-stratified ($N^2 < 2x10^{-5}$ rad^2 s^{-2}) (Fig. 2). Conversely, all stations sampled during the summer cruise were strongly stratified with $N^2 > 5x10^{-5}$ rad^2 s^{-2} (Fig. 2) and had relatively consistent and shallow mixed layer depths which ranged from 18 to 46 m. Water temperature displayed a latitudinal gradient in the spring with surface temperatures ranging from 18.6°C in the south to 8.9°C in the north (Fig. 3A). Temperatures were higher during the summer and displayed strong gradients with both latitude and depth (Fig. 3E). Temperatures were highest in the surface waters ranging from 22.8°C between 30-33°N to 13.0°C between 60-63°N. A prominent thermocline (i.e., rapid decrease in temperature from surface mixed layer to cold deep water) persisted over the latitudinal range of the cruise. Salinity demonstrated similar latitudinal trends as temperature for both seasons; however, vertical depth gradients were only apparent in the south during the summer (Fig. 3B, F). Resultant from the vertical and latitudinal gradients in temperature and salinity, seawater density exhibited strong gradients with depth and geographical location (Fig. 3C, G). During the spring, extrapolated vertical mixing coefficients (K_T) were low (10^{-3} m^2 s^{-1}) in the surface waters of southern stations indicating weak vertical mixing, while at the northern stations strong vertical mixing extended down to 100 m, indicating a well-mixed water column as a result of strong wind prior to our arrival (Jurado et al. 2012a). Vertical mixing was on average one order of magnitude lower in the summer and showed a sharp decline (from 10^{-5} to 10^{-1} m^2 s^{-1}) towards the bottom of the mixed layer (Fig. 3D). Around 33°N, vertical mixing in the mixed layer stabilized around 10^{-3} m^2 s^{-1} (i.e., $\log_{10}(K_T) \approx -3$) until 59°N, where values in the upper 20 m declined by an order of magnitude to 10^{-4} m^2 s^{-1}.

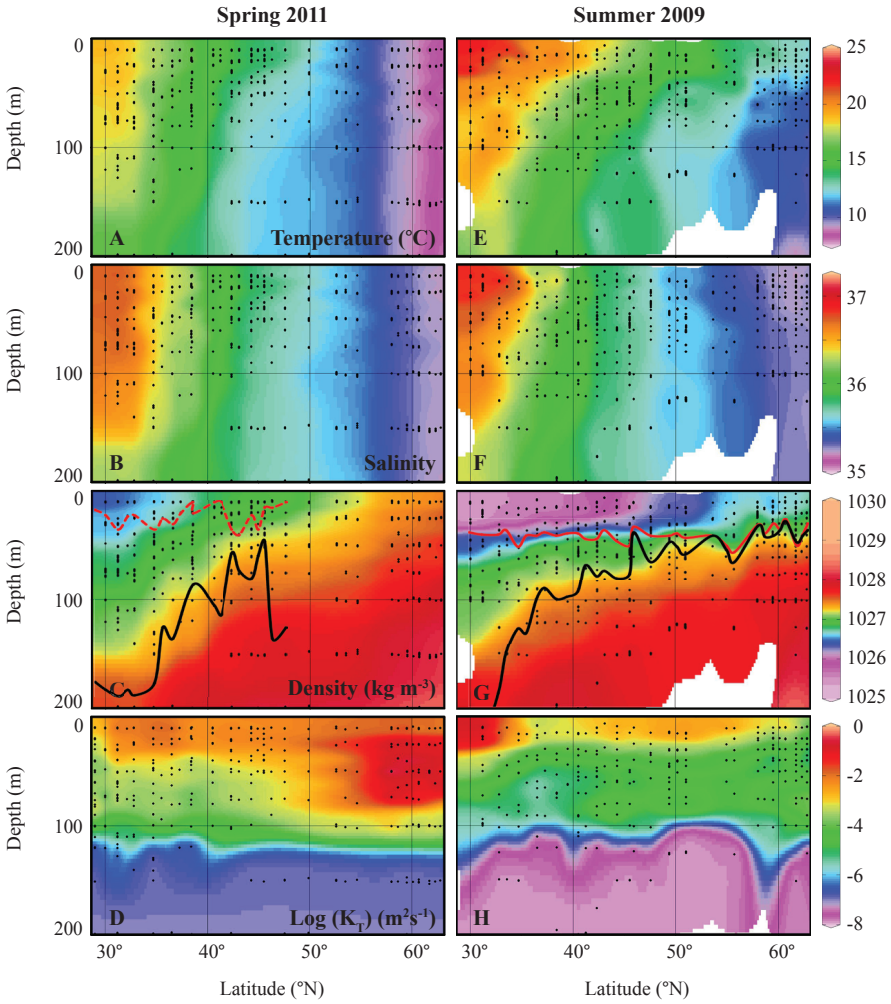

Figure 3. Physical characteristics of water column sampled over the spring (A-D) and summer (E-H) STRATIPHYT cruises. Black dots indicate measurement points. Lines in figure panels C & G represent the pycnocline depth (red) and nutricline depth (black). The pycnocline depth was defined as the depth with the greatest $\Delta\rho/\Delta z$. The dotted line indicates a weak pycnocline in spring. Nutricline depth was defined by a 5 µM change in NO_3^- relative to surface values. In the northern region during the spring, the pycnocline and nutricline were not detected within the depths sampled, and consequently the lines end at the station where they were last detected.

Nitrate (NO_3^-) and phosphate (PO_4^{3-}) were highly depleted (below detection limit) in the mixed layer up to 40°N in the spring and 45°N in summer. A steep nutricline for NO_3^- and PO_4^{3-} was observed in the stratified regions during both seasons (Fig. 4A, E and B, F, respectively). In the north (58-63°N) spring surface concentrations averaged 11.5 µM NO_3^- and 0.8 µM PO_4^{3-}, whereas lower average concentrations were observed during summer, i.e., 1.2 and 0.14 µM for NO_3^- and PO_4^{3-}, respectively. In

the spring, nitrite (NO_2^-) concentration was maximal at the base of the nutricline (around 0.4 µM), which also corresponded closely with Z_{eu}. In the summer, NO_3^- concentrations were typically below the detection limit south of 49°N, with the highest concentration (0.8 µM) around 60 m just north of 50°. Ammonium concentrations in spring were typically below detection limit except between 41-55°N, and in summer north of 49°N. Overall N:P ratio in the Z_m in the spring averaged 8.8±6.5 south and 15.4±1.2 north of 45°N and averaged 10.6±9.4 in summer.

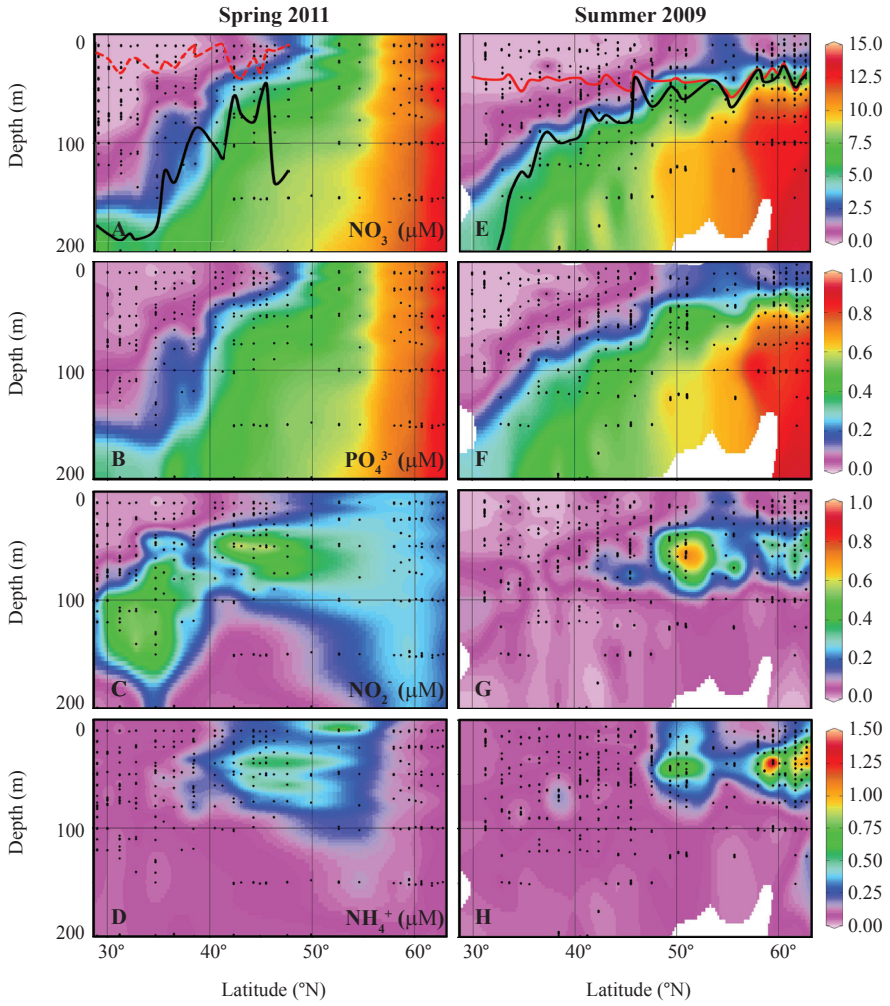

Figure 4. Nutrient profiles of water column sampled over the spring (A-D) and summer (E-H) STRATIPHYT cruises. Black dots indicate measurement points. Lines in figure panels A & E represent the pycnocline depth (red) and nutricline depth (black). The pycnocline depth was defined as the depth with the greatest $\Delta\rho/\Delta z$. The dotted line indicates a weak pycnocline in spring. Nutricline depth was defined by a 5 µM change in NO_3^- relative to surface values. In the northern region during the spring, the pycnocline and nutricline were not detected within the depths sampled, and consequently the lines end at the station where they were last detected.

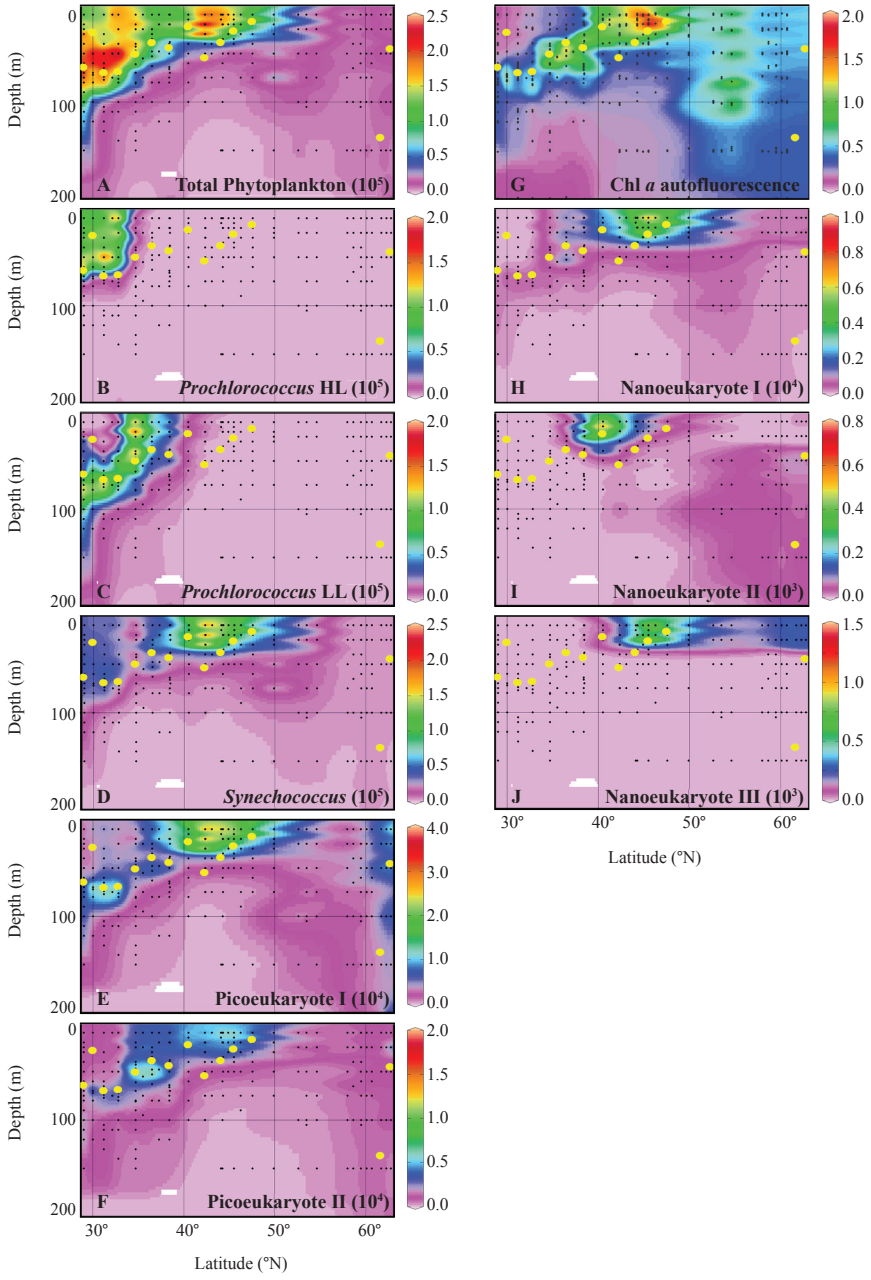

Figure 5. ODV plots of the abundance (ml^{-1}) of total phytoplankton < 20 µm (A), photosynthetic picoprokaryotes (B-D), picoeukaryotes (E and F), HPLC calibrated Chl a autofluorescence (mg m^{-3}) and nanoeukaryote abundance determined by flow cytometry during the spring STRATIPHYT cruise. Black dots indicate measurement points. Yellow dots illustrate Z_m; the absence of yellow points between 50-60°N is due to Z_m deeper than maximal sampling depth. During the spring, Nano IV was not detected.

Phytoplankton data

Spring

In the spring, pico-sized photoautotrophs dominated the total phytoplankton enumerated by FCM (on average 97%) (Fig. 5). Total phytoplankton abundance was highest in the south and declined towards the north, corresponding to strong vertical mixing and deep mixing depths (Fig. 3). South of 35°N, *Prochlorococcus* populations were the numerically dominant phytoplankton groups (Fig. 5B,C). North of 35°N, phytoplankton became confined to the surface mixed layer and the abundance of eukaryotic phytoplankton increased. Nano I-IV maxima occurred between 35-50°N, which corresponded with a peak in Chl *a* (Fig. 5G). The Chl *a* depth profile showed clearly the deep mixing of phytoplankton north of 50°N (Z_m = 225-311 m). At the northernmost stations, calm weather conditions prior to measurements allowed the water column to become more stabilized, reducing mixing depths to < 200 m, and permitting abundances of Pico I and II, and Nano III to once again increase in the surface layer.

Oligotrophic areas as defined by nutrient concentrations (i.e., NO_3^- ≤ 0.13 µM and PO_4^{3-} ≤ 0.03 µM; van de Poll et al. 2013) or Chl *a* concentrations (< 0.07 mg Chl m^{-3}) extended to 40°N. Phytoplankton pigment analysis showed that the deep chlorophyll maximum (DCM) of the most oligotrophic region (28-35°N) was largely comprised of *Prochlorococcus*, prasinophytes, pelagophytes and *Synechococcus* (25, 20, 16 and 10%, respectively; Fig. 6). The surface (0-40 m) peak in Chl *a* between 40-50°N (Fig. 6G) was largely made up by haptophytes (53%; Fig. 6D), diatoms (13%; Fig. 6H) and prasinophytes (12%; Fig. 6C). North of 50°N, haptophytes and diatoms dominated until 58°N where cryptophytes became one of the major groups with an average 22% of total (as compared to 19% for haptophytes and diatoms, Fig. 6). Microscopic analysis showed that diatoms of northern stations consisted mainly of large *Bacteriastrum* sp. (> $1.0x10^3$ cells l^{-1}), with pennates (i.e., *Nitzschia longissima*) and small *Chaetoceros* spp. in lower numbers. Haptophytes consisted of cf. *Emiliania huxleyi* as well as *Phaeocystis*-like cells. The diatom composition at southern stations consisted of the small *Pseudonitzschia* cf. *delicatissima*, and short *Leptocylindrus mediterraneus* chains.

Depth-integrated (0-250 m) cellular C from FCM phytoplankton counts (< 20 µm diameter) ranged between 1.2 and 1.7 g C m^{-2} at the southern oligotrophic stations (Fig. 7A). Pico-sized phytoplankton (pico-prokaryotes and –eukaryotes) comprised the largest percentage (57 - 92%) of the algal C biomass of this region (Fig. 7B). Of the cyanobacteria, both *Synechococcus* and *Prochlorococcus* LL had

an equal contribution to algal biomass of (on average) 24% with a much lower contribution from *Prochlorococcus* HL of 8.5%. Depth-integrated algal C was maximum around 46°N at 7.4 g C m^{-2} and ranged between 1.01 - 2.57 g C m^{-2} in the non-stratified regions of the north (> 50°N; Fig. 7A). Nanoeukaryotes (Nano I-IV) were responsible for the greatest proportion of total algal biomass in the northern half of the transect, comprising between 74 and 92% (Fig. 7B). S-N differences in the contribution of Pico I and II to group-specific C were not present and Pico II made up the largest percentage (on average 69%) over the entire latitudinal range. Nano I comprised all of the nanoeukaryotic phytoplankton C until 42°N, while in non-stratified stations (> 50°N) groups II and III were responsible for the majority of cellular C (53 - 82%).

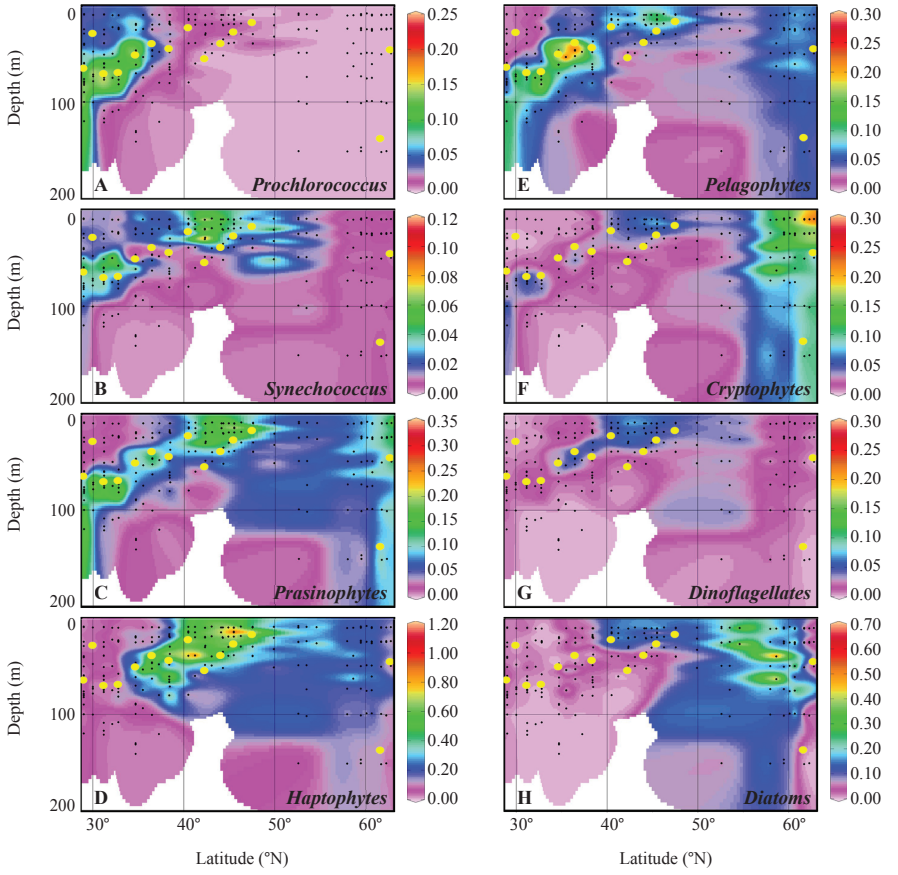

Figure 6. ODV plots of relative Chl a concentrations (mg Chl a m^{-3}) of taxonomic groups determined by HPLC pigment analysis using CHEMTAX identification following the spring STRATIPHYT cruise. Black dots indicate measurement points. Yellow dots indicate Z_m.

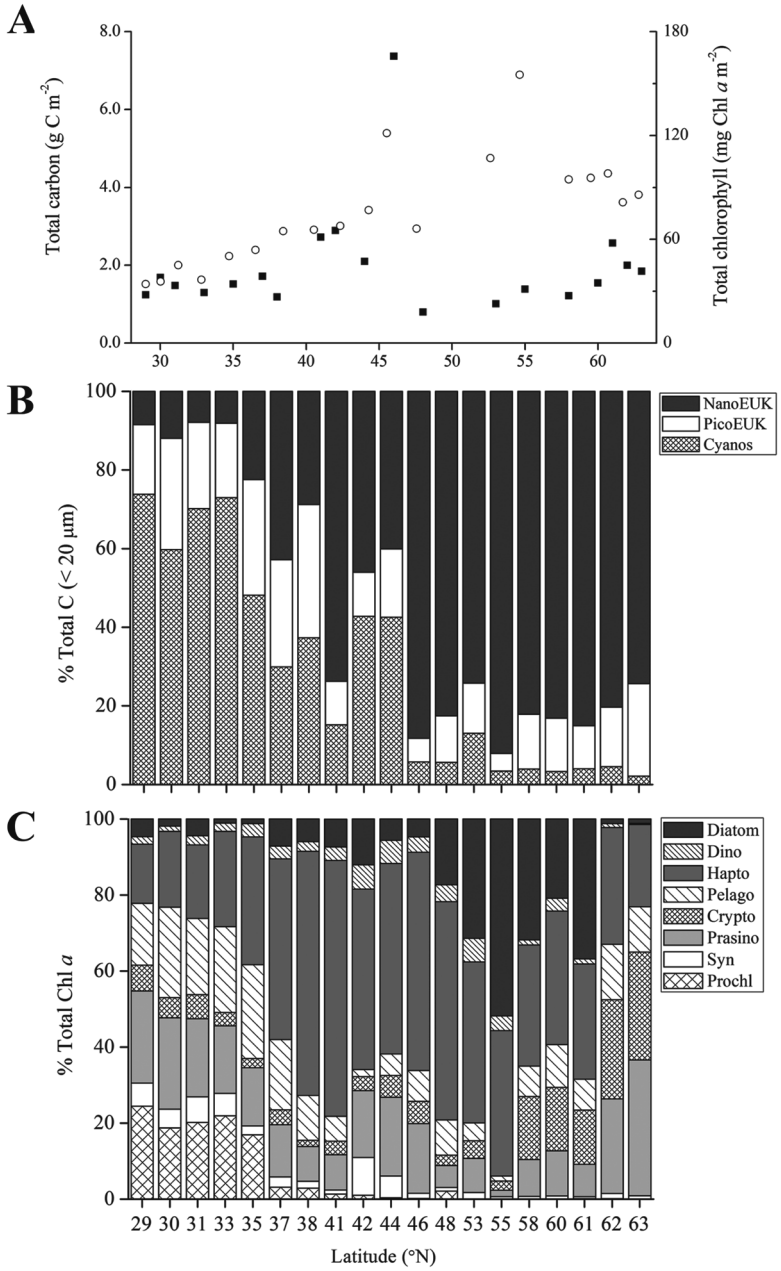

Figure 7. Depth-integrated total phytoplankton carbon (< 20 µm) determined from flow cytometry (closed squares) and depth-integrated total Chl a determined from HPLC calibrated Chl a autofluorescence (open circles) (A), the percent composition of depth-integrated (0 - 250 m) total carbon (< 20 µm) (B), and taxonomic composition of depth-integrated (0 - 250 m) total Chl a determined by HPLC pigment analysis using CHEMTAX identification (C) during the spring.

Depth-integrated Chl *a* concentration varied between 36 - 66 mg Chl *a* m^{-2} in southern oligotrophic region (< 40°N) (Fig. 7A). The taxonomic composition of depth integrated Chl *a* in this region was primarily comprised of haptophytes (37%), pelagophytes (18%), prasinophytes (17%) and *Prochlorococcus* (14%) (Fig. 7C). North of 40°, depth-integrated Chl *a* ranged between 62-155 mg m^{-2}, with an average concentration of 94 mg m^{-2}. Haptophytes (40%), diatoms (19% up to 50% at station 55) and cryptophytes (12%) were important contributors to total Chl *a* of mesotrophic regions. Similar to depth integrated carbon, Chl *a* demonstrated a peak in concentrations at 46°N reaching concentrations of 121 mg m^{-2} (Fig. 7A). The relaxation of the vertical mixing in the northern most stations reduced the contribution of diatoms again to 13%.

Summer

Similar to spring, pico-sized phytoplankton dominated, i.e., 95% of the total phytoplankton enumerated by FCM (Fig. 8). In contrast to spring, however, phytoplankton abundances were lower in the surface layer (0 - 25 m). South of 45°N, total abundance was maximal ($1.6\pm0.4x10^5$ cells ml^{-1}) below the Z_m and tapered off towards the depth of the nutricline, which is characteristic for a deep-chlorophyll maximum (DCM). The prokaryote *Prochlorococcus* was the most abundant member of the phytoplankton community in the southern most region (31 - 33°N), with the HL population dominating the upper 0 - 55 m surface waters (92%; Fig. 8B) and the LL population being more abundant at the DCM (93%; Fig. 8C). The DCM shallowed with latitude, giving over to a surface maximum north of 45°N. This also marked the upper boundary of oligotrophic areas, which occurred 5° north compared to the spring. When the base of the Z_m was situated above the nutricline, picoeukaryotic photoautotrophs became maximal in the surface waters and *Prochlorococcus* disappeared. The cyanobacteria *Synechococcus* spp. showed highest abundances in the north ($7.0\pm0.4x10^5$ ml^{-1}; Fig 8D) numerically dominating the photosynthetic community < 20 µm (making up 74% of the total counts). The abundance of the picoeukaryotic phytoplankton increased north of 38°N with Pico II being more dominant in the northern half of the transect (Fig. 8E, F). Chl *a* and cell size increased towards the north (Fig. 8G - K). Although nanoeukaryotic phytoplankton abundance was relatively low, their larger cell size contributed substantially to Chl *a* autofluorescence (Fig. 8G). The abundance of the different nanoeukaryotic phytoplankton groups was inversely related to cell size, whereby the largest sized Nano III and IV were the least abundant and found only in the surface waters of the most northern stations (Fig. 8K).

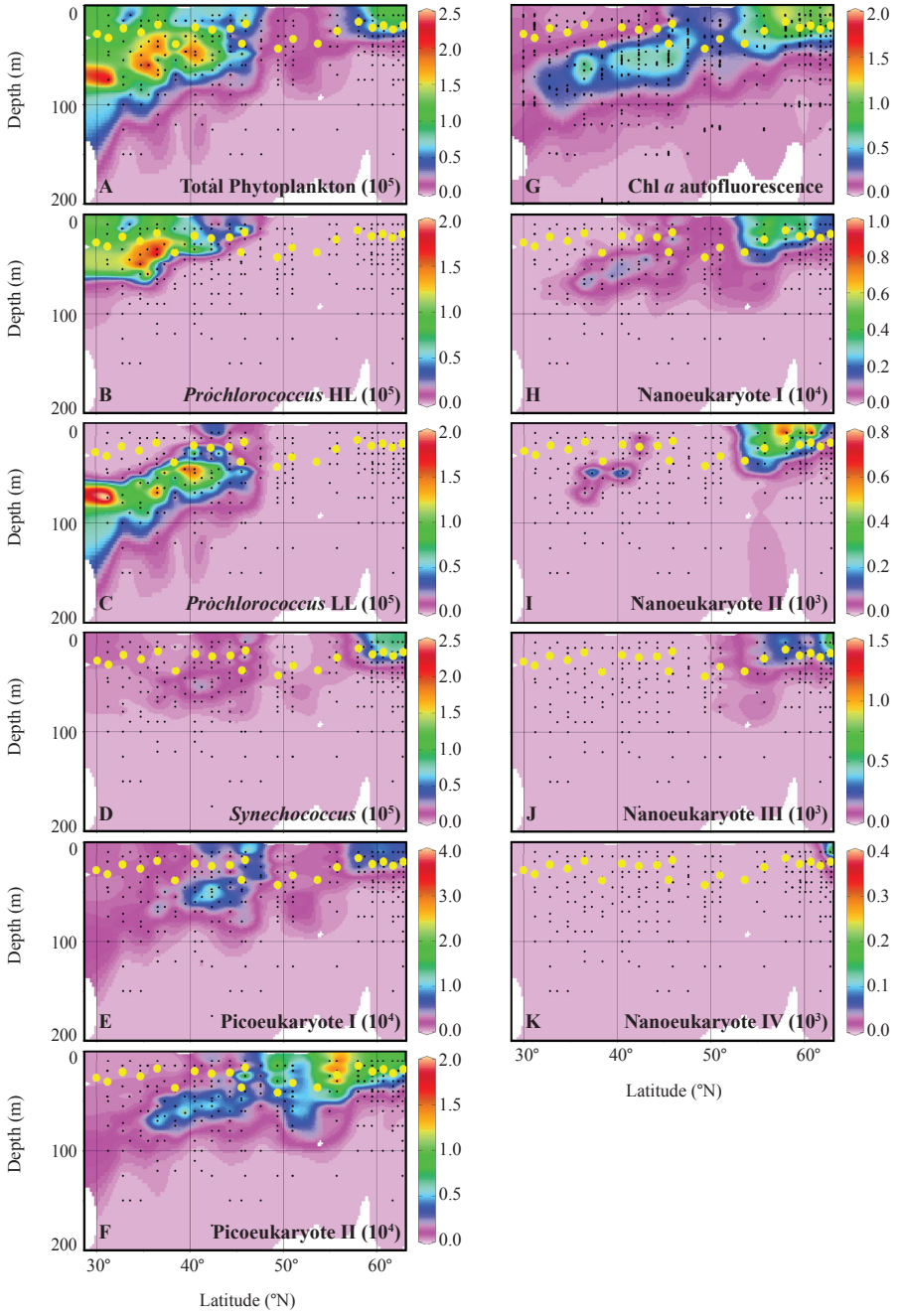

Figure 8. ODV plots of the abundance (ml^{-1}) of total phytoplankton < 20 µm (A), photosynthetic picoprokaryotes (B - D), picoeukaryotes (E and F), HPLC calibrated Chl a autofluorescence (mg m^{-3}) and nanoeukaryote abundance determined by flow cytometry during the summer STRATIPHYT cruise. Black dots indicate measurement points. Yellow dots illustrate Z_m.

Phytoplankton pigment analysis (Fig. 9) indicated that northern surface populations were largely made up by haptophytes (around 48%), followed by prasinophytes (16%), pelagophytes (12%), and dinoflagellates (12%). *Synechococcus*, cryptophytes and diatoms also had pigment concentration maxima in these regions (> 60°N), but contributed very little to the total community composition (≤ 5%) (Fig. 9). In the strongly stratified southern stations (30 - 45°N), haptophytes remained a principal component of the algal community based on Chl *a* (average 24%; Fig. 9D) with *Prochlorococcus*, prasinophytes, pelagophytes and *Synechococcus* contributing 23, 17, 12 and 12%, respectively (Fig. 9A - D). Microscopic analysis revealed that diatoms of the northern stations consisted of pennates with *Nitzschia longissima* and *Pseudonitzschia* cf. *delicatissima* as main representatives. The haptophyte *Phaeocystis* increased towards the north reaching maximum cell numbers at 58°N of around $2x10^3$ cells ml^{-1}. In contrast to spring, *Phaeocystis* was primarily found in colonial form with colony bladders often colonized by other phytoplankton species as well as heterotrophs (i.e., dinoflagellates, ciliates).

Integrated over depth (0 - 250 m), cellular C from FCM counts were 2 to 4-fold lower in the summer compared to spring and ranged between 0.33 and 2.53 g C m^{-2} (Fig. 10), with the lowest values (max. 0.81 g C m^{-2}) in the oligotrophic south (< 45°N). Pico-sized phytoplankton dominated (70 - 97%) the south, with cyanobacteria contributing an average of 19, 29 and 8% for *Prochlorococcus* HL, *Prochlorococcus* LL and *Synechococcus*, respectively. As latitude increased nanoeukaryotes (Nano I - IV) became responsible for the greatest proportion of total carbon biomass (with *Synechococcus* and picoeukaryotic phytoplankton sharing the residual 15 - 40%). Depth-integrated Chl *a* biomass was also 2-fold lower in summer compared to spring, varying between 17 - 27 mg Chl *a* m^{-2} in oligotrophic regions (Fig. 10A), with *Prochlorococcus*, haptophytes and prasinophytes as the principal contributors (24, 24, and 18%, respectively). Moving north, the importance of haptophytes increased (Fig. 10C). Similar to that of total organic C, the highest values for total Chl *a* were found north of 55°N with maximum values of around 43 mg Chl *a* m^{-2} (Fig. 10A).

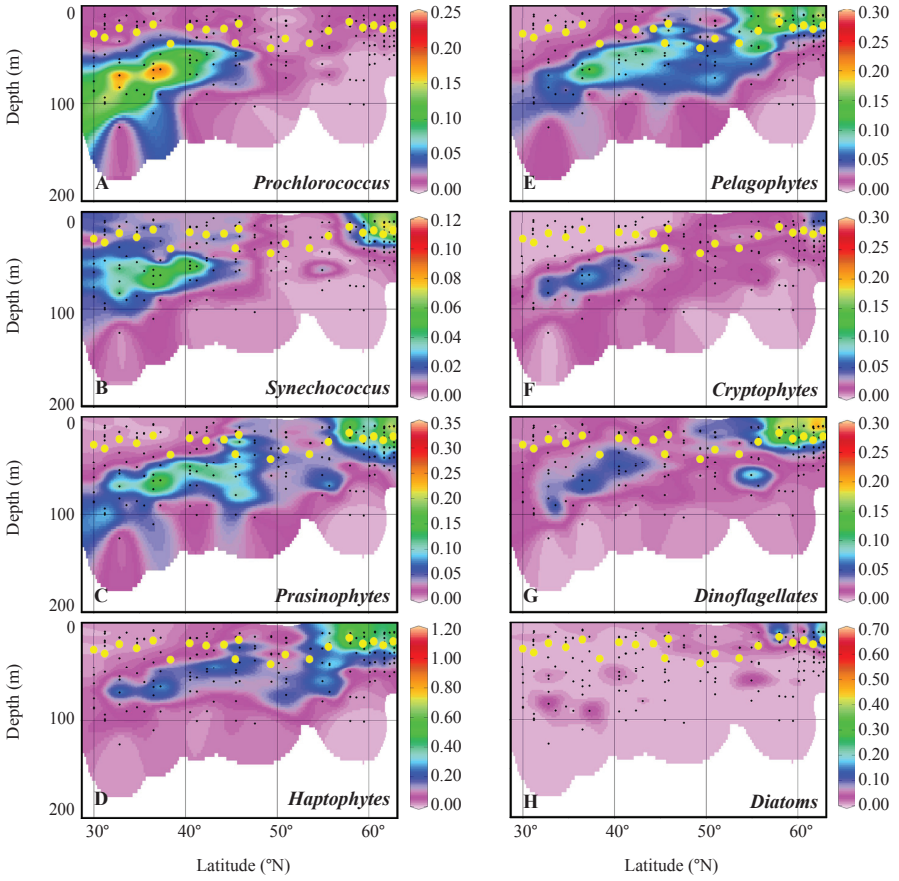

Figure 9. ODV plots of taxonomic group specific Chl a concentrations (mg Chl a m^{-3}:based on CHEMTAX) for the STRATIPHYT summer cruise. Black dots indicate measurement points. Yellow dots indicate Z_m.

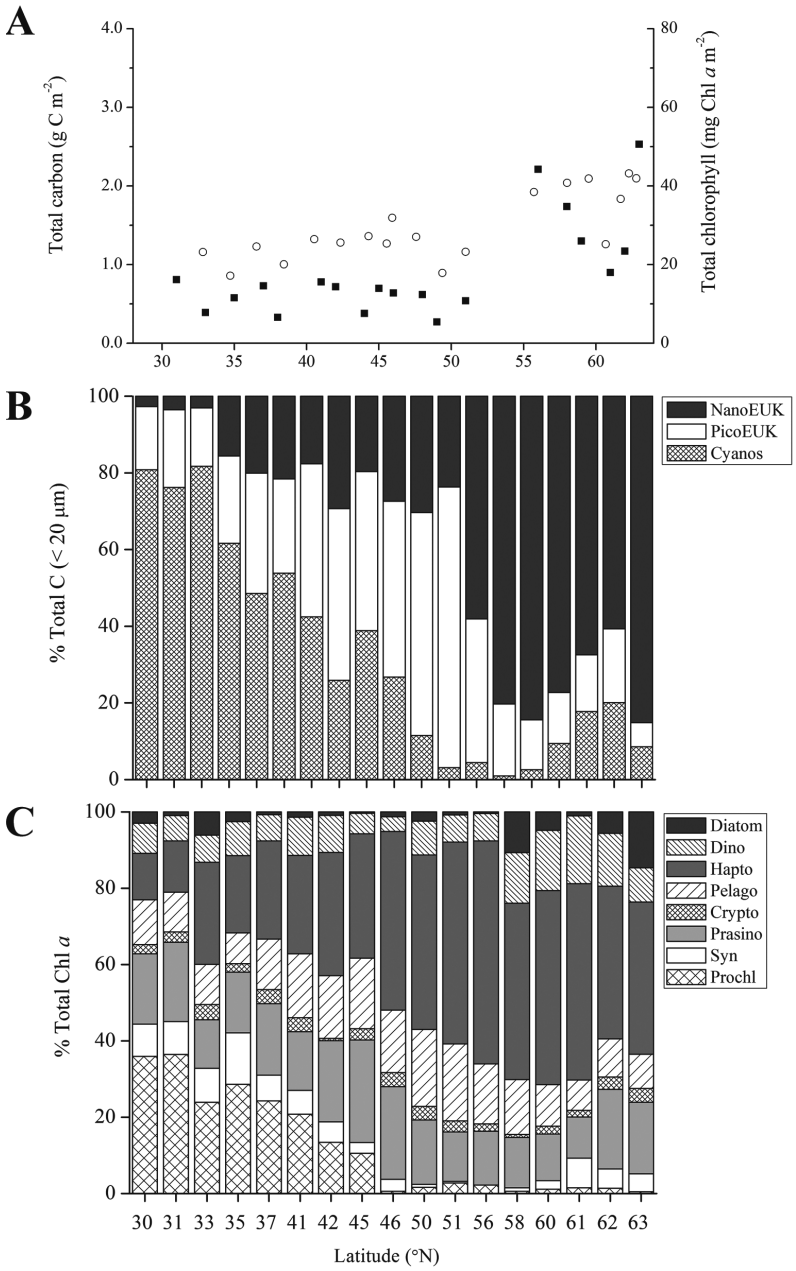

Figure 10. (A) Depth-integrated total phytoplankton carbon (cell size < 20 µm) determined by flow cytometry (closed squares) and depth-integrated total Chl a determined by HPLC calibrated Chl a autofluorescence. (B) Community composition based on total phytoplankton carbon determined by flow cytometry. (C) Community composition based on total Chl a determined by HPLC pigment analysis using CHEMTAX identification during summer.

Statistical Analysis

Redundancy analysis (RDA) was used to investigate relationships between the phytoplankton community composition (red lines) and the environmental variables (blue lines in Fig. 11). Lines in the RDA triplots pointing in the same direction are positively correlated, while lines pointing in opposite directions are negatively correlated. In addition, the triplots show how stratification and depth level (symbols) are associated with the community composition and environmental variables. We note that the RDA does not show NO_3^- and temperature as environmental variables, because PO_4^{3-} was collinear with NO_3^- (Pearson correlation: $r = 0.99$, $p < 0.001$) and salinity was collinear with temperature ($r = 0.87$, $p < 0.001$). In Fig. 11A, the phytoplankton community composition is quantified in terms of carbon based on FCM analysis. The eigenvalues (obtained from model output) revealed that the first two axes of this RDA triplot explained 27% and 12% of the variation in the dataset. The main environmental variables contributing to the formation of the first axis were PO_4^{3-} and depth level, while the second axis was mainly influenced by salinity (temperature) and PO_4^{3-} (NO_3^-). *Prochlorococcus* C was associated with relatively high salinity/temperature environments with deep Z_{eu} and low nutrient concentrations, all characteristic of stratified subtropical waters (Fig. 9A). Moreover, the HL and LL *Prochlorococcus* populations were differentiated by the stronger association of the HL population to higher salinity/temperature and lower association with the Z_m (Fig. 11A). *Synechococcus* and Pico I and II were associated with the Z_m of relatively high temperature, low nutrient waters. Conversely, nanoeukaryotic phytoplankton C was correlated to the Z_m of relatively lower temperature, higher nutrient and shallow Z_{eu} waters.

When the phytoplankton was quantified as percentage distribution of total C, multivariate analysis showed that the first two axes of the RDA explain approximately 16% and 10% of the variation in the data, respectively (Fig. 11B). The most influential variables to the formation of the first axis were again PO_4^{3-} and salinity, while the second axis was mainly influenced by depth layer, Z_m/Z_{eu}, NO_2^- and stratification level. *Prochlorococcus*, *Synechococcus* and picoeukaryotic phytoplankton had high contributions to total C at high salinity/temperature, low nutrient environments and were differentiated by higher contributions of *Prochlorococcus* HL, and *Synechococcus* in the Z_m. Nano I - IV on the other hand showed higher contributions to total C in relatively lower temperature, higher nutrient environments. A higher proportion of Nano I cellular C was associated with BZ_m environments with higher N:P ratios, while Nano II and III were associated with Z_m environments with high Z_m/Z_{eu}.

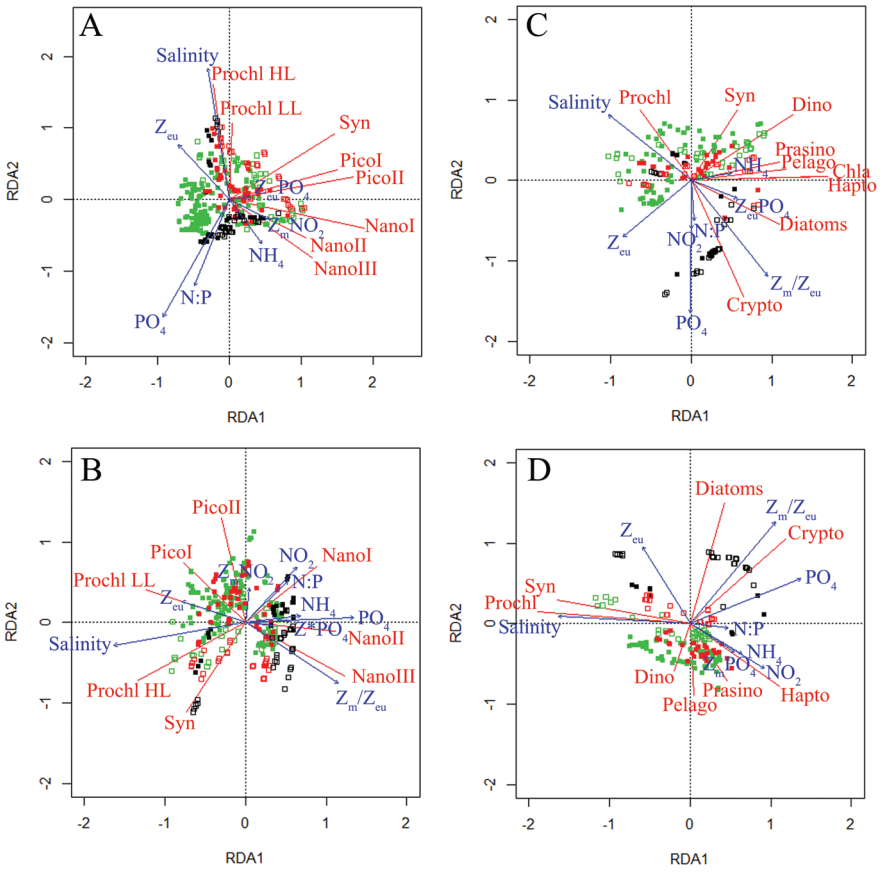

Figure 11. Redundancy Analysis (RDA) correlation triplots of phytoplankton community composition (in red) in relation to environmental variables (in blue). The community composition is quantified in terms of (A) phytoplankton carbon (cell size < 20 µm) and (B)[1] percentual distribution of phytoplankton carbon, both calculated from the FCM counts, (C) Chlorophyll a concentration and (D) percentual distribution of the Chlorophyll a concentration, both calculated from the pigment analysis using CHEMTAX. Data represented in figures are compiled from both the summer and spring STRATIPHYT cruises. Symbols illustrate from what stratification and depth level the samples originated from; according to depth layer (open = mixed layer and closed = below mixed layer) and colored according to stratification level (green = strongly stratified, red =weakly stratified, and black = non-stratified stations). Environmental variables: Z_{eu} = euphotic zone depth, N:P = ratio of DIN to PO_4^{3-}, Z_m/Z_{eu} = ratio of mixed layer depth to euphotic zone depth, $Z_mPO_4 = PO_4^{3-}$ flux into the mixed layer, $Z_{eu}PO_4 = PO_4^{3-}$ flux into the euphotic zone, $Z_mNO_2 = NO_2^-$ flux into the mixed layer, and [1] $Z^*PO_4 = Z_{eu}PO_4$ & Z_mPO_4, which are labeled together to improve readability as arrows overlay one another. PO_4^{3-} is collinear with NO_3^- (Pearson correlation: r = 0.99, p < 0.001) and salinity is collinear with temperature (r = 0.9, p < 0.001). Biological variables: Prochl HL = Prochlorococcus high-light, Prochl LL = Prochlorococcus low-light), Syn = Synechococcus, Pico = picoeukaryotes, Nano = nanoeukaryotes, Dino = dinoflagellates, Hapto = haptophytes, Prasino = prasinophytes, Crypto = cryptophytes, and Pelago = pelagophytes.

When the community composition was based on pigment analysis and expressed in terms of Chl *a*, the first two axes of the RDA explained 29% and 13% of the variation (Fig. 11C). The first axis was mainly influenced by Z_m/Z_{eu} and inversely by salinity. The second axis was mainly formed by PO_4^{3-} and stratification. *Prochlorococcus*-specific Chl *a* was associated with strongly stratified waters with high temperature/salinity, low nutrients and low Z_m/Z_{eu}. Conversely, cryptophytes and diatoms were related to relatively colder, non-stratified waters with high availability of nutrients and high Z_m/Z_{eu}. Total Chl *a* and the remaining taxonomic groups were moderately coupled to warmer stratified waters with shallow $Z_{eu.}$

When the community composition was based on the percentage distribution of the Chl *a* concentration, the first two axes of the RDA explained 24% and 15% of the variation in the data (Fig. 11D). The first axis was mainly influenced by salinity (negative correlation) and PO_4^{3-}, and the second axis by depth layer and Z_m/Z_{eu}. Diatoms and cryptophytes were related to non-stratified waters with relaxed nutrient limiting conditions and a higher Z_m/Z_{eu} ratio. Conversely, an increased contribution of dinoflagellates were associated with BZ_m of stations with stronger stratification and fewer nutrients. Consistent with phytoplankton C analysis, the contribution of *Prochlorococcus* was associated with high temperature/salinity and low nutrient environments. However, one notable difference was the high correlation of *Synechococcus* with *Prochlorococcus*, which is absent from FCM measurements. Finally, prasinophytes, haptophytes and pelagophytes were related to BZ_m of stations characterized by lower temperatures/salinities, higher nutrients and shallower Z_{eu}.

Overall, environmental data explained 47, 37, 52 and 56% of the total variation in phytoplankton group-specific C, %C, Chl *a* and %Chl *a*, respectively (Table 2). As ecological data are general quite noisy and consequently can never be expected to yield a high value of R^2 (Legendre and Legendre 1998), these values provide confidence that the major patterns within the data have been captured by the RDA model. Variance partitioning demonstrated that stratification level alone explained 4 - 8% of the variation (Table 2). Therefore, inclusion of Brunt-Väisälä frequency (N^2) as an index of stratification increased the variation explained by the environmental data. Running the models without considering nutrient flux into the surface waters demonstrated nearly equivalent R^2, demonstrating equal coverage by both models. However, in the case of size composition data, inclusion of nutrient flux reduced the explained variation partitioned to stratification level (from 7.4 to 4.1%).

Table 2. Variance decomposition of the RDA models in Fig. 11A - D, based on phytoplankton carbon (< 20 µm), percentual distribution of phytoplankton carbon (%Carbon), Chlorophyll *a* concentration and percentual distribution of the Chlorophyll *a* concentration (%Chl *a*). RDA models were partitioned to show the percentage of variance explained by all the variables, all the variables except stratification level, stratification level alone, shared variance (collinearity present in the model which could not be removed) and residual variance (remaining variance not explained by the model).

		Variance (%)			
Component	Source	A. Carbon	B. %Carbon	C. Chl *a*	D. %Chl *a*
	All variables	47.09	37.26	51.50	55.71
A	All variables – stratification level	41.52	28.36	42.31	40.02
B	stratification level	6.91	4.07	6.98	7.84
C	Shared	-1.35	4.83	2.21	7.85
D	Residual	52.91	62.74	48.50	44.29

Discussion

Comparing CHEMTAX and FCM

FCM provides detailed information about abundance and size structure of the phytoplankton community. In contrast, pigment analysis with CHEMTAX provides information regarding taxonomic composition including larger-sized algae that are typically missed by FCM, but lacks information regarding cell abundances and is unable to differentiate size differences within taxonomic groups (Uitz et al. 2006; Uitz et al. 2008). These differences between CHEMTAX and FCM analysis became apparent when comparing depth-integrated Chl *a* (obtained from pigment analysis) and total phytoplankton C (obtained by FCM) across the two seasons. While the results of both methods were tightly coupled during the summer (when small-sized phytoplankton dominated), they deviated from each other in the spring where there was a higher contribution of larger-sized phytoplankton taxa north of 40°N. Using a fixed carbon : chlorophyll ratio of 50 (Brown et al. 1999), carbon determined from pigments and FCM counts were in good agreement during the summer and within oligotrophic regions during the spring. However, Chl *a* carbon concentrations were up to 5-fold higher during the spring in the well-mixed high latitude regions, which coincided with a higher presence of larger diatoms species as seen from both CHEMTAX and microscopy observations. In spite of methodological differences between FCM and pigment analysis, combining the two methods permitted us to examine how changes in vertical stratification affected both the size structure and taxonomic composition of

phytoplankton communities, and provided additional information regarding the potential taxonomic groups comprising different phytoplankton size classes. Based on our results, we recommend that future studies combine FCM and CHEMTAX analysis, and use size-fractionation for both FCM and HPLC samples. This would provide useful information regarding the size composition of taxa as well as of numerically abundant groups, and may improve taxonomic identification of FCM groups.

Although phytoplankton pigment analysis confirmed the general spatial distributions of the prokaryotic phytoplankton, there were some notable discrepancies compared to FCM. Pigments specific for *Prochlorococcus* were low for near-surface samples despite their high numerical abundance determined by FCM. This indicates either a low cellular concentration of this pigment in the HL population or could indicate a reduced retention of small cells during filtration. The smaller average cell diameter of *Prochlorococcus* HL in this study (i.e., 0.6 μm) compared to the LL population (i.e., 0.7 - 0.8 μm) does support the latter. Photoacclimation related changes are most strongly observed in photoprotective pigments (e.g., diadinoxanthin, diatoxanthin and violaxanthin, antheraxanthin and zeaxanthin) and subsequently these pigments show steep vertical gradients within the water column. As a result, photoprotective pigments are to be avoided when using CHEMTAX analysis when alternative pigments are available. In addition, photoacclimation can alter cellular pigment concentrations. Pigments specific for *Prochlorococcus* (e.g. divinyl chlorophyll *a*) have been shown to be reduced by 37 - 50% in high-light acclimated cells of *Prochlorococcus* HL ecotype eMED45 (Partensky et al. 1993). In addition, a twelve fold difference in cellular divinyl chlorophyll *a* concentrations has been reported for field populations of *Prochlorococcus* (Partensky et al. 1999b). This suggests that the variability in carbon to chlorophyll *a* ratios of this species may be a main cause for the discrepancy between flow cytometry derived carbon data and pigment based data from CHEMTAX found for oligotrophic stations. Pigment and FCM based detection of *Synechococcus* also revealed inconsistencies. Detection of *Synechococcus* based on zeaxanthin indicated a higher signature in the DCM regions compared to detection based on phycoerythrin fluorescence as determined by FCM. Phycoerythrin has higher specificity than zeaxanthin and is most likely a better indicator for this genus, however, it is not soluble in acetone, excluding its utility in CHEMTAX due to the pigment extraction method. The use of two separate pigments for the identification of this taxa does not appear to permit a direct comparison between these two methods.

Phytoplankton distributions in relation to vertical stratification

Pico-sized phytoplankton, and particularly cyanobacteria, dominated the total phytoplankton abundance and biomass (< 20 μm) of the stratified southern region, consistent with evidence for the importance of this size class for the production in warm, low nutrient waters (Partensky et al. 1996; Maranon et al. 2000; Perez et al. 2006; Uitz et al. 2006). *Prochlorococcus* was the main photosynthetic prokaryotic group, with the northern edge of its distributions closely matching oligotrophic boundaries (varying from 42 to 48°N between spring and summer). The contribution to total biomass (i.e., 32 and 48% in the spring and summer, respectively) and geographic distribution of *Prochlorococcus* are both in the upper range of those reported in the literature (i.e., 21 - 43% and typically found 40°S - 45°N; Johnson et al. 2006; Whitton and Potts 2012). The northern edge of the distribution of *Prochlorococcus* coincided closely with a reduction in temperature, supporting evidence that temperature acts as a critical factor regulating the distribution of this genus (Johnson et al. 2006; Zinser et al. 2007; Flombaum et al. 2013). The ubiquity and numerical dominance of *Prochlorococcus* within stratified oligotrophic waters of the world's oceans is thought to be a consequence of both genetic streamlining (and subsequent reduction in cell size), and diversity in genomic evolution within the genus facilitating a range of niche partitioning (Partensky and Garczarek 2010). Coherent with this hypothesis, FCM distinguished two distinct populations of *Prochlorococcus* (Johnson et al. 2006; Zinser et al. 2007) that dominated at different depths and latitudes. *Prochlorococcus* HL dominated over *Synechococcus* 2-fold under conditions of strong stratification, which was reversed under weak stratification. The prevalence of *Prochlorococcus* LL changed very little between the two seasons, which is consistent with a study revealing a shift from cyanobacteria with a small genome (i.e., *Prochlorococcus* HLII) to those with a larger genome (i.e., *Prochlorococcus* LL and *Synechococcus*) with increased vertical mixing in the upper 10 m water column (Bouman et al. 2011). The dominance of *Synechococcus* over *Prochlorococcus* following deep winter mixing is often attributed to the inability of *Prochlorococcus* to utilize the increased nitrate concentrations (Whitton and Potts 2012). Our results suggest that future alterations in stratification will also play a role in governing phylogeography within the unicellular cyanobacterial populations.

The geographical distribution of *Synechococcus* extended further northwards than that of *Prochlorococcus*, illustrating the broader temperature range of *Synechococcus* (Moore et al. 1995; Partensky et al. 1999a; Peloquin et al. 2013). Recently, it was suggested that the ability of *Synechococcus* spp. to regulate photochemistry over a

range of temperatures through temperature dependent association of phycobilisome (PBS) to the different photosystems may explain the larger geographic range of this group relative to *Prochlorococcus* spp., which lack PBS (Mackey et al. 2013). However, we also provide evidence that nutrients are important in regulating the abundance of *Synechococcus*. *Synechococcus* demonstrated lowest abundances in oligotrophic regions and abundances were maximal where the nutricline was the shallowest. In addition, the contribution of *Synechococcus* to total C was higher in the spring (up to 43% compared to 25% in the summer). The success of this genus under high nutrient concentrations is in line with maximal abundances observed in the highly productive upwelling regions where concentrations can be up to a magnitude higher than in oceanic regions (Morel 1997; Whitton and Potts 2012). The predominance of pico-sized cells in the oligotrophic regions is often attributed to a competitive advantage over larger phytoplankton in low nutrient environments afforded by the lower nutrient requirements, small diffusion boundary layers and large surface area per unit volume of small cell size (Raven 1986; Chisholm 1992; Finkel et al. 2010). This is consistent with our finding of nutrients as an important agent for phytoplankton size structure. Aside from picoprokaryotic autotrophs, eukaryotic haptophytes (ranging 23 - 36% between summer and spring), prasinophytes (17 - 19%) and pelagophytes (13 - 18%) substantially contributed to depth integrated Chl *a* concentration within the oligotrophic regions. This concurs with evidence from literature that these groups are important components of picoeukaryotic phytoplankton communities, and can represent up to 35% of total picoeukaryotic cells (Guillou et al. 2004; Liu et al. 2009; Jardillier et al. 2010). As even tiny haptophytes may produce organic plate scales this genus may play a significant role in the biological pump of stratified areas (Liu et al. 2009).

Vertical stratification affects the phytoplankton dynamics by regulating the availability of light and nutrients to phytoplankton in the ocean (Behrenfeld et al. 2006; Huisman et al. 2006; Hoegh-Guldberg and Bruno 2010). Our results demonstrate that incorporating an index for stratification, such as Brunt-Väisälä frequency (N^2), can improve the explained variation in phytoplankton data, both in terms of cell size and taxonomic composition. The underlying reason is probably that this stratification index captures the impact of stratification on various physicochemical processes, such as the flux of nutrients into the euphotic zone. Our finding that the inclusion of nutrient flux into the surface waters reduces the variation explained by stratification level, without improving the overall coverage of the model, tends to support this hypothesis.

In general, phytoplankton biomass and primary production (van de Poll et al. 2013) were highest where the nutricline was the shallowest, suggesting a strong coupling between the nutricline, the rate of nutrient supply to the euphotic zone and the photosynthetic performance of phytoplankton in the North Atlantic Ocean (Behrenfeld et al. 2006). The depth of the nutricline was closely tied to the shift in dominance of key phytoplankton genera and size classes. Besides the switch in the dominant cyanobacterial group from *Prochlorococcus* in waters with a deep nutricline to *Synechococcus* in waters with a shallow nutricline, a switch from picoeukaryotic to nanoeukaryotic phytoplankton as the principal contributors to C biomass < 20 µm was also apparent during both seasons. Nutricline depth is thought to reflect nutrient supply into the upper mixed layer and when implemented as a proxy for water column stability has successfully explained basin-scale changes in the relative contribution of diatoms and coccolithophores to total phytoplankton biomass (Cermeño et al. 2008). We found that the maximum group-specific Chl *a* concentrations for prasinophytes, haptophytes, phototrophic dinoflagellates and some extent pelagophytes (summer) coincided with the shallowing of the nutricline. The association of phototrophic dinoflagellates and pelagophytes with higher nutrient concentrations is not surprising considering their relatively large cell size (Irigoien et al. 2004; Edwards et al. 2012). Dinoflagellates, however, were most prevalent during the summer in the north, which agrees with their tendency to favor warmer waters, with shallower Z_m, higher mean irradiance and reduced vertical mixing (Irwin et al. 2012). Although the current study estimated phytoplankton contribution based on taxon-specific pigments, the mixotrophic capacity of some phytoplankton species cannot be excluded. Haptophytes, prasinophytes, cryptophytes and dinoflagellates have all been shown to contain mixotrophic representatives (McKie-Krisberg and Sanders 2014; Unrein et al. 2014). Such nutritional flexibility would provide a competitive advantage under low light and low (inorganic) nutrient regimes.

During the spring the water column north of 53°N remained non-stratified, which resulted in the vertical uniformity of temperature, salinity, density and nutrients in the upper 200 m. This is consistent with observations of high latitude regions of the Atlantic remaining well mixed in the upper 200 m between December to April (van Aken 2000). Deep mixing and high turbulence in the north (> 50°N) during the spring dispersed cells to depths greater than 200 m, reducing phytoplankton abundance and phytoplankton pigment concentrations. However, when integrated over the sampled water column, these northern stations demonstrated the highest Chl *a* concentrations per m^2 indicating high phytoplankton C biomass in these regions,

despite being dispersed over hundreds of meters. Chlorophyll *a* concentrations specific for diatoms and cryptophytes were greatest in these homogeneously mixed waters. The association of these taxa with higher macronutrient concentrations is consistent with their lower half-saturation constants for nutrient uptake and nutrient-limited growth (Litchman et al. 2006; Irwin et al. 2012).

Modeling the phytoplankton composition of future oceans

The current study provides a high-resolution mesoscale description of physical, chemical and biological (phytoplankton community composition and size) characteristics in the upper 200 m water column along a stratification gradient in the Northeast Atlantic Ocean during two periods of stratification. The multivariate approach identified ocean stratification as one of the key drivers for the distribution and separation of different phytoplankton taxa and size classes. Here we elaborate on key features of our results pertinent to biogeochemical and ecological modeling studies of the present and future oceans.

Models can improve our understanding and prediction of climate-induced changes in plankton community composition, primary production and associated biogeochemical cycles. During recent years, interesting model approaches have been developed in which a broad spectrum of phytoplankton "species" with different growth parameters and different responses to light and nutrients become self-organized into distinct biogeographical communities across the global ocean (e.g. Follows et al. 2007). The predictions of these models critically depend on questions as to which traits best differentiate phytoplankton functional groups and which environmental variables regulate primary production and community structure (Behrenfeld et al. 2006; Irwin et al. 2012). In this sense, predictions of how the ocean ecosystem will respond to climate change are still limited by a lack of information regarding which taxonomic groups are essential and what environmental controls determine the distribution and succession of these taxonomic groups (Falkowski et al. 2000; Litchman et al. 2006; Finkel et al. 2010).

The classification of phytoplankton functional types (PFT) is dependent on the scientific question to be addressed by the model (Claustre 1994; Falkowski et al. 1998; Le Quéré et al. 2005). For biogeochemical models based on functional taxa, PFT should, for example (i) play a specific biogeochemical role, (ii) be defined by distinct set of physiological, environmental or nutritional requirements which regulate biomass and productivity, and (iii) be of quantitative importance in some regions of the ocean (Le Quéré et al. 2005). Based on this definition, we

can classify our phytoplankton groups into several PFTs. Picocyanobacteria and picoeukaryotic phytoplankton were highest in abundance and showed largest contributions to phytoplankton biomass in stratified waters ($N^2 > 2x10^{-5}$ rad^2 s^{-2}). The picocyanobacteria PFT could be distinguished by a higher association with warm temperatures and high water clarity (deep Z_{eu}), and conversely, the picoeukaryote PFT by a higher association with nutrient flux into the surface layers ($Z_m NO_2$ and $Z_{eu}PO_4$). Furthermore, our results indicate that in addition to temperature and light (as recently reported by Flombaum et al. 2013) incorporation of the N:P ratio and vertical turbulence structure of the water column will be useful to distinguish between the niches of the different picocyanobacterial populations (*Prochlorococcus* HL, *Prochlorococcus* LL and *Synechococcus*). Another main PFT, the diatoms, were distinguished by their association with the surface layers of non-stratified waters ($N^2 < 2x10^{-5}$ rad^2 s^{-2}), colder water temperatures, higher nutrient concentrations and higher potential for light limitation. There is some evidence for successional shifts in dominance between diatoms and cryptophytes (Moline et al. 2004; Mendes et al. 2013) and several studies have reported selective grazing by different zooplankton species on either diatoms or cryptophytes (Cotonnec et al. 2001; Haberman et al. 2003; Liu et al. 2010), which may advocate for an additional PFT for cryptophytes. If warranted, our analysis suggests that this cryptophyte PFT can be distinguished from diatoms by the closer association of cryptophytes with high Z_m/Z_{eu} and conversely of diatoms with high $Z_{eu}PO_4$.

Some models combine autotrophic dinoflagellates, prasinophytes, pelagophytes and haptophytes together into one or more 'mixed phytoplankton' PFT due to their lack of a distinguishable biochemical role or absence of bloom formation (Le Quéré et al. 2005). In our data, these taxa were distinguished from other phytoplankton by their high contribution to total Chl *a* in the DCM of the stratified waters. However, dinoflagellates were associated to waters with a shallow Z_{eu}, whereas the haptophytes and prasinophytes showed a higher association with NH_4^+ and NO_2^-. This is consistent with observations that haptophytes contain several species (e.g., *Phaeocystis* spp., *Emiliania huxleyi*) that have relatively high NH_4^+ uptake rates (Tungaraza et al. 2003) and can develop dense blooms in N-rich parts of the global ocean (Schoemann et al. 2005; Lacroix et al. 2007). In addition, haptophytes have the ability to produce organic or calcium carbonate plates (Not et al. 2012) and may thereby directly contribute to the biological pump (with obvious contributions by calcifying coccolithophores). Mixotrophy, although not exclusive to this taxa (McKie-Krisberg and Sanders 2014; Unrein et al. 2014), toxicity and

bioluminescence can be distinct traits of relevance to dinoflagellates. Hence, dinoflagellates, prasinophytes and haptophytes play different ecological roles (Not et al. 2012) and our data show that they can be discriminated as separate PFTs.
Taxonomic groups often contain different size classes, which may provide more information than PFT discrimination based on taxonomic affiliation alone. Cell size is an important feature to consider from an ecological point of view, as it affects numerous functional characteristics of phytoplankton (Litchman et al. 2007). Important advances have therefore been made by models that predict phytoplankton community composition from the size structure of the constituent species (Armstrong 1994; Baird and Suthers 2007; Ward et al. 2012). This matches our data, where we find clear differences in the biogeographical distributions of picocyanobacteria (0.6 - 1 µm), picoeukaryotic phytoplankton (1 - 2 µm), small nanoeukaryotic phytoplankton (Nano I; 6 - 8 µm) and larger nanoeukaryotes (Nano II & III; 8 - 9 µm). However, our results also show that phytoplankton groups of similar size (such as the different picocyanobacterial groups) may still respond very differently to the environmental conditions. Hence, size structure alone is not sufficient to describe community structure, and other physiological traits (e.g., pigment composition, nutrient preferences, motility) need to be considered as well.
Our results indicate that in addition to the classic environmental factors temperature, nutrients and light, incorporation of the vertical turbulence structure of the water column is likely to improve existing models. In our statistical analysis, vertical mixing was described by two parameters, the Brunt-Väisälä frequency N^2 and mixing depth Z_m, which improved differentiation between the different PFT. In mathematical models vertical mixing is usually described by partial differential equations for the transport of heat, solutes and phytoplankton cells. Indeed, models and field experiments have shown that changes in vertical turbulent mixing can have dramatic impacts on the species composition of phytoplankton communities (Huisman et al. 2004; Jäger et al. 2008; Ryabov et al. 2010). However, numerical simulation of vertical mixing processes at a sufficiently high resolution to capture the vertical redistribution of phytoplankton species is computationally quite demanding (Huisman and Sommeijer 2002; Pham Thi et al. 2005), and computational power is one of the main limiting factors for their application in ecosystem models of the global ocean. Yet, vertical mixing processes provide a vital link between changes in the global climate, thermal stratification of the water column, nutrient fluxes and the growth, spatial distribution and species composition of phytoplankton communities (Follows and Dutkiewicz 2001; Jöhnk et al. 2008; Dutkiewicz et al.

2013). Hence, our results stress the need for an improved description of the vertical turbulence structure in global ocean models if we want to capture this vital link.

Conclusions

While we are confident that the major trends within our data were captured by the RDA models, not all of the variation in the distribution of phytoplankton over the Northeast Atlantic could be explained. The remaining variation could be an indication for the importance of loss factors to structuring phytoplankton communities. Loss factors including viral lysis and grazing can be substantial enough to counterbalance growth of natural phytoplankton communities (K. D. A. Mojica unpubl.)(Behrenfeld and Boss 2014). As the fate of photosynthetically fixed carbon is essential for ecosystem efficiency and the functioning of the biological pump, more information is needed to understand how climate-induced changes in stratification will alter these loss processes.

Our results support the prediction that future increases in temperature will expand the geographic range of *Prochlorococcus* as oligotrophic areas continue to expand northward (Polovina et al. 2008; Flombaum et al. 2013). Furthermore, the data indicate that the increased contribution of *Prochlorococcus* to C biomass will occur at the expense of *Synechococcus* spp., leading to alterations in phylogeography within the unicellular cyanobacterial populations. Besides alterations to picocyanobacteria populations, future increases in (summer) stratification will likely increase the contribution of haptophytes, prasinophytes and pelagophytes in the northern region of the North Atlantic relative to cryptophytes and diatoms.

Acknowledgements

The STRATIPHYT project was supported by the division for Earth and Life Sciences Foundation (ALW), with financial aid from the Netherlands Organization for Scientific Research (NWO). We thank the captains and shipboard crews of R/V Pelagia and scientific crews during the cruises. We acknowledge the support of NIOZ-Marine Research Facilities (MRF) on-shore and on-board. Furthermore, we thank Harry Witte (Department Biological Oceanography, NIOZ, Texel) for his assistance with the initial statistical analysis.

References

Armstrong RA (1994) Grazing limitation and nutrient limitation in marine ecosystems: steady state solutions of an ecosystem model with multiple food chains. Limnology and Oceanography 39: 597-608

Baird ME, Suthers IM (2007) A size-resolved pelagic ecosystem model. Ecological Modelling 203: 185-203

Beaugrand G (2009) Decadal changes in climate and ecosystems in the North Atlantic Ocean and adjacent seas. Deep-Sea Research, Part II 56: 656-673

Behrenfeld MJ, Boss ES (2014) Resurrecting the ecological underpinnings of ocean plankton blooms. Annual Review of Marine Science 6: 167-194

Behrenfeld MJ, O'Malley RT, Siegel DA, McClain CR, Sarmiento JL, Feldman GC, Milligan AJ, Falkowski PG, Letelier RM, Boss ES (2006) Climate-driven trends in contemporary ocean productivity. Nature 444: 752-755

Bouman HA, Ulloa O, Barlow R, Li WKW, Platt T, Zwirglmaier K, Scanlan DJ, Sathyendranath S (2011) Water-column stratification governs the community structure of subtropical marine picophytoplankton. Environmental Microbiology Reports 3: 473-482

Brainerd KE, Gregg MC (1995) Surface mixed and mixing layer depths. Deep-Sea Research, Part I 42: 1521-1543

Brown SL, Landry MR, Barber RT, Campbell L, Garrison DL, Gowing MM (1999) Picophytoplankton dynamics and production in the Arabian Sea during the 1995 Southwest Monsoon. Deep-Sea Research, Part II 46: 1745-1768

Cermeño P, Dutkiewicz S, Harris RP, Follows M, Scholfield O, Falkowski PG (2008) The role of nutricline depth in regulating the ocean carbon cycle. Proceedings of the National Academy of Sciences of the United States of America 105: 20344-20349

Chisholm SW (1992) Phytoplankton size. In: Falkowski PG, Woodhead AD (eds) Primary Productivity and Biogeochemical Cycles. Plenum Press

Claustre H (1994) The trophic status of various oceanic provinces as revealed by phytoplankton pigment signatures. Limnology and Oceanography 39: 1206-1210

Collins M, Knutti R, Arblaster J, Dufresne J-L, Fichefet T, Friedlingstein P, Gao X, Gutowski WJ, Johns T, Krinner G, Shongwe M, Tebaldi C, Weaver AJ, Wehner M (2013) Long-term climate change: projections, commitments and irreversibility. In: Stocker TF, Qin D, Plattner G-K, Tignor M, Allen SK, Boschung J, Nauels A, Xia Y, Bex V, Midgley PM et (eds) Climate change 2013: The physical science basis. Contribution of working group I to the fifth assessment report of the Intergovernmenal Panel on Climate Change. Cambridge University Press

Cotonnec G, Brunet C, Sautour B, Thoumelin G (2001) Nutritive value and selection of food particles by copepods during a spring bloom of *Phaeocystis* sp. in the English Channel, as determined by pigment and fatty acid analyses. Journal of Plankton Research 23: 693-703

Daufresne M, Lengfellner K, Sommer U (2009) Global warming benefits the small in aquatic ecosystems. Proceedings of the National Academy of Sciences of the United States of America 106: 12788-12793

Dawson B, Spannagle M (2008) The Complete Guide to Climate Change. Taylor & Francis.

Deser C, Blackmon ML (1993) Surface climate variations over the North Atlantic ocean during winter: 1900-1989.Journal of Climate 6: 1743-1753

Doney, SC, Ruckelshaus M, Duffy JE, Barry JP, Chan F, English CA, Galindo HM, Grebmeier JM, Hollowed AB, Knowlton N, Polovina J, Rabalais NN, Sydeman WJ (2012) Climate change impacts on marine ecosystems. Annual Review of Marine Science 4: 11-37

Dutkiewicz S, Scott JR, Follows MJ (2013) Winners and losers: ecological and biogeochemical changes in a warming ocean. Global Biogeochemical Cycles 27: 463-477

Edler L, Elbrächter M (2010) The Utermöhl method for quantitative phytoplankton analysis. In: Karlson B, Cusack C, Bresnan E (eds) Microscopic and Molecular Methods for Quantitative Phytoplankton Analysis. Intergovernmental Oceanographic Commission of © UNESCO

Edwards KF, Thomas MK, Klausmeier CA, Litchman E (2012) Allometric scaling and taxonomic variation in nutrient utilization traits and maximum growth rate of phytoplankton. Limnology and Oceanography 57: 554-566

Edwards M, Richardson AJ (2004) Impact of climate change on marine pelagic phenology and trophic mismatch. Nature 430: 881-884

Falkowski P, Scholes RJ, Boyle E, Canadell J, Canfield D, Elser J, Gruber N, Hibbard K, Hogberg P, Linder S, Mackenzie FT, Moore III B, Pedersen T, Rosenthal Y, Seitzinger S, Smetacek V, Steffen W, (2000) The global carbon cycle: a test of our knowledge of Earth as a system. Science 290: 291-296

Falkowski PG, Barber RT, Smetacek V (1998) Biogeochemical controls and feedbacks on ocean primary production. Science 281: 200-206

Finkel ZV, Beardall J, Flynn KJ, Quigg A, Rees TAV, Raven JA (2010) Phytoplankton in a changing world: cell size and elemental stoichiometry. Journal of Plankton Research 32: 119-137

Flombaum P, Gallegos JL, Gordillo RA, Rincon J, Zabala LL, Jiao N, Karl DM, Li WKW, Lomas MW, Veneziano D, Vera CS, Vrugt JA, Martiny AC (2013) Present and future global distributions of the marine cyanobacteria *Prochlorococcus* and *Synechococcus*. Proceedings of the National Academy of Sciences of the United States of America 110: 9824-9829

Follows MJ, Dutkiewicz S, Grant S, Chisholm SW (2007) Emergent biogeography of microbial communities in a model ocean. Science 315: 1843-1846

Follows MJ, Dutkiewicz SW (2001) Meteorological modulation of the North Atlantic spring bloom. Deep-Sea Research, Part II 49: 321-344

Furrer R, Nychka D, Sain S (2012) fields: Tools for spatial data. http://CRAN.R-project.org/package=fields

Garrison DL, Gowing MM, Hughes MP, Campbell L, Caron DA, Dennett MR, Shalapyonok A, Olson RJ, Landry MR, Brown SL, Liu HB, Azam F, Steward GF, Ducklow HW, Smith DC (2000) Microbial food web structure in the Arabian Sea: a US JGOFS study. Deep-Sea Research, Part II 47: 1387-1422

Grasshoff K (1983) Determination of nitrate. In: Grasshoff K, Erhardt M, Kremeling K (eds) Methods of Seawater Analysis. Verlag Chemie

Gregg WW, Conkright ME, Ginoux P, O'Reilly JE, Casey NW (2003) Ocean primary production and climate: global decadal changes. Geophysical Research Letters 30: 1809. doi: 10.1029/2003GL016889

Guillou L, Eikrem W, Chrétiennot-Dinet MJ, Le Gall F, Massana R, Romari K, Pedros-Alio C, Vaulot D (2004) Diversity of picoplanktonic prasinophytes assessed by direct nuclear SSU rDNA sequencing of environmental samples and novel isolates retrieved from oceanic and coastal marine ecosystems. Protist 155: 193-214

Haberman KL, Ross RM, Quetin LB (2003) Diet of the Antarctic krill (*Euphausia superba* Dana): II. Selective grazing in mixed phytoplankton assemblages. Journal of Experimental Marine Biology and Ecology 283: 97-113

Helder W, De Vries RTP (1979) An automatic phenol-hypochlorite method for the determination of ammonia in sea and brackish water. Netherlands Journal of Sea Research 13: 154-160

Hilligsøe KM, Richardson K, Bendtsen J, Sorensen LL, Nielsen TG, Lyngsgaard MM (2011) Linking phytoplankton community size composition with temperature, plankton food web structure and sea-air CO_2 flux. Deep-Sea Research, Part I 58: 826-838

Hoegh-Guldberg,O, Bruno JF (2010) The impact of climate change on the world's marine ecosystems. Science 328: 1523-1528

Hooker SB, Van Heukelem L, Thomas CS, Claustre H, Ras J, Schluter L, Clementson L, vanderLinde D, Eker-Develi E, Berthon J-F, Barlow R, Sessions H, Ismail H, Perl J (2009) The third SeaWiFS HPLC analysis round-robin experiment (SeaHARRE-3). NASA Technical Memorandum 2009-215849. Greenbelt: NASA Goddard Space Flight Center

Houry S, Dombrowsky E, De May P, Minster J-F (1987) Brunt-Väisälä frequency and rossby radii in the South Atlantic. Journal of Physical Oceanography17: 1619-1626

Huisman J, Sharples J, Stroom JM, Visser PM, Kardinaal WEA, Verspagen JMH, Sommeijer B (2004) Changes in turbulent mixing shift competition for light between phytoplankton species. Ecology 85: 2960-2970

Huisman J, Sommeijer B (2002) Population dynamics of sinking phytoplankton in light-limited environments: simulation techniques and critical parameters. Journal of Sea Research 48: 83-96

Huisman J, Thi NNP, Karl DM, Sommeijer B (2006) Reduced mixing generates oscillations and chaos in the oceanic deep chlorophyll maximum. Nature 439: 322-325

Huisman J, Van Oostveen P, Weissing FJ (1999) Critical depth and critical turbulence: two different mechanisms for the development of phytoplankton blooms. Limnology and Oceanography 44: 1781-1787

Irigoien X, Huisman J, Harris RP (2004) Global biodiversity patterns of marine phytoplankton and zooplankton. Nature 429: 863-867

Irwin AJ, Nelles AM, Finkel ZV (2012) Phytoplankton niches estimated from field data. Limnology and Oceanography 57: 787-797

Jäger CG, Diehl S, Schmidt GM (2008) Influence of water-column depth and mixing on phytoplankton biomass, community composition, and nutrients. Limnology and Oceanography 53: 2361-2373

Jardillier L, Zubkov MV, Pearman J, Scanlan DJ (2010) Significant CO_2 fixation by small prymnesiophytes in the subtropical and tropical northeast Atlantic Ocean. The ISME Journal 4: 1180-1192

Jöhnk KD, Huisman J, Sharples J, Sommeijer B, Visser PM, Stroom JM (2008) Summer heatwaves promote blooms of harmful cyanobacteria. Global Change Biology 14: 495-512

Johnson ZI, Zinser ER, Coe A, McNulty NP, Woodward EMS, Chisholm SW (2006) Niche partitioning among *Prochlorococcus* ecotypes along ocean-scale environmental gradients. Science 311: 1737-1740

Jurado E, Dijkstra HA, Van Der Woerd HJ (2012a) Microstructure observations during the spring 2011 STRATIPHYT-II cruise in the northeast Atlantic. Ocean Science 8: 945-957

Jurado E, Van Der Woerd HJ, Dijkstra HA (2012b) Microstructure measurements along a quasi-meridional transect in the northeastern Atlantic Ocean. Journal of Geophysical Research 117: C04016. doi: 10.1029/2011JC007137

Koroleff F (1969) Direct determination of ammonia in natural waters as indophenol blue. Coun. Meet. int. Coun. Explor. Sea **C.M.-ICES/C:** 9

Lacroix G, Ruddich K, Gypens N, Lancelot C (2007) Modelling the relative impact of rivers (Scheldt/Rhine/Seine) and Western Channel waters on the nutrient and diatoms/*Phaeocystis* distributions in Belgian waters (Southern North Sea). Continental Shelf Research 27: 1422-1446

Le Quéré C, Harrison SP, Prentice IC, Buitenhuis ET, Aumont O, Bopp L, Claustre H, Da Cunha LC, Geider R, Giraud X, Klaas C, Kohfeld KE, Legendre L, Manizza M, Platt T, Rivkin RB, Sathyendranath S, Uitz J, Watson AJ, Wolf-Gladrow D (2005) Ecosystem dynamics based on plankton functional types for global ocean biogeochemistry models. Global Change Biology 11: 2016-2040

Legendre P, Legendre L (1998) Numerical ecology, 2nd English ed. Elsevier Science BV

Levitus S, Antonov JI, Boyer TP, Stephens C (2000) Warming of the world ocean. Science 287: 2225-2229

Li WKW (2002) Macroecological patterns of phytoplankton in the northwestern North Atlantic Ocean. Nature 419: 154-157

Litchman E, Klauseier CA, Miller JR, Schofield OM, Falkowski PG (2006) Multi-nutrient, multi-group model of present and future oceanic phytoplankton communities. Biogeosciences 3: 585-606

Litchman E, Klausmeier CA, Schofield OM, Falkowski PG (2007) The role of functional traits and trade-offs in structuring phytoplankton communities: scaling from cellular to ecosystem level. Ecology Letters10: 1170-1181

Liu H, Probert I, Uitz J, Claustre H, Aris-Brosou S, Frada M, Not F, De Vargas C (2009) Extreme diversity in noncalcifying haptophytes explains a major pigment paradox in open oceans. Proceedings of the National Academy of Sciences of the United States of America 106: 12803-12808

Liu HB, Chen MR, Suzuki K, Wong CK, Chen BZ (2010) Mesozooplankton selective feeding in subtropical coastal waters as revealed by HPLC pigment analysis. Marine Ecology Progress Series **407:** 111-123.

Mackey, K. R. M., A. Paytan, K. Caldeira, A. R. Grossman, D. Moran, M. Mcilvin, and M. A. Saito. 2013. Effect of temperature on photosynthesis and growth in marine *Synechococcus* spp. Plant Physiol. 163: 815-829

Mackey MD, Mackey DJ, Higgins HW, Wright SW (1996) CHEMTAX - A program for estimating class abundances from chemical markers: application to HPLC measurements of phytoplankton. Marine Ecology Progress Series 144: 265-283

Mahadevan A, D'Asaro E, Lee C, Perry MJ (2012) Eddy-driven stratification initiates North Atlantic spring phytoplankton blooms. Science 337: 54-58

Maranon E, Holligan PM, Varela M, Mourino B, Bale AJ (2000) Basin-scale variability of phytoplankton biomass, production and growth in the Atlantic Ocean. Deep-Sea Research, Part I 47: 825-857

McKie-Krisberg ZM, Sanders RW (2014) Phagotrophy by the picoeukaryotic green algal *Micromonas*: implications for Arctic Oceans. The ISME Journal 8: 1953-1961

Meehl GA, Stocker TF, Collins WD, Friedlingstein P, Gaye AT, Gregory JM, Kitoh A, Knutti R, Murphy JM, Noda A, Raper SCB, Watterson IG, Weaver AJ, Zhao Z-C (2007) Global climate projections. In: Solomon S, Qin D, Manning M, Chen Z, Marquis M, Averyt KB, Tignor M, Miller HL (eds) Climate change 2007: The physical science basis. Contribution of working group I to the fourth assessment report of the Intergovernmental Panel on Climate Change. Cambridge University Press

Mendes CRB, Tavano VM, Leal MC, De Souza MS, Brotas V, Garcia CAE (2013) Shifts in the dominance between diatoms and cryptophytes during three late summers in the Bransfield Strait (Antarctic Peninsula). Polar Biology 36: 537-547

Mitra A, Flynn KJ (2005) Predator-prey interactions: is 'ecological stoichiometry' sufficient when good food goes bad? Journal of Plankton Research 27: 393-399

Moline MA, Claustre H, Frazer TK, Schofield O, Vernet M (2004) Alteration of the food web along the Antarctic Peninsula in response to a regional warming trend. Global Change Biology 10: 1973-1980

Moore LR, Chisholm SW (1999) Photophysiology of the marine cyanobacterium *Prochlorococcus*: Ecotypic differences among cultured isolates. Limnology and Oceanography 44: 628-638

Moore LR, Goericke R, Chisholm SW (1995) Comparative physiology of *Synechococcus* and *Prochlorococcus* - influence of light and temperature on growth, pigments, fluorescence and absorptive properties. Marine Ecology Progress Series 116: 259-275

Morel A (1997) Consequences of a *Synechococcus* bloom upon the optical properties of oceanic (case 1) waters. Limnology and Oceanography 48: 1746-1754

Murphy J, Riley JP (1962) A modified single solution method for the determination of phosphate in natural waters. Analytica Chimica Acta 27: 31-36

Not F, Siano R, Kooistra WHCF, Simon N, Vaulot D, Probert I (2012) Diversity and ecology of eukaryotic marine phytoplankton. In: Gwenaël P (ed) Advances in Botanical Research. Academic Press

Oksanen J, Blanchet FG, Kindt R, Legendre P, Minchin PR, O'Hara RB, Simpson GL, Solymos, P, Stevens MHH, Wagner H (2013) vegan: Community ecology package. http://CRAN.R-project.org/package=vegan

Partensky F, Blanchot J, Lantoine F, Neveux J, Marie D (1996) Vertical structure of picophytoplankton at different trophic sites of the tropical northeastern Atlantic Ocean. Deep-Sea Research, Part I 43: 1191-1213

Partensky F, Blanchot J, Valout D (1999a) Differential distribution and ecology of *Prochlorococcus* and *Synechococcus* in oceanic waters: a review. Bulletin de l'Institut océanographique (Monaco) 19: 457-475

Partensky F, Garczarek L (2010) *Prochlorococcus*: advantages and limits of minimalism. Annual Review of Marine Science 2: 305-331

Partensky F, Hess WR, Vaulot D (1999b) *Prochlorococcus*, a marine photosynthetic prokaryote of global significance. Microbiology and Molecular Biology Reviews 63: 106-127

Partensky, F., N. Hoepffner, W. K. W. Li, O. Ulloa, and D. Vaulot. 1993. Photoacclimation of *Prochlorococcus* sp. (Prochlorophyta) strains isolated from the North Atlantic and the Mediteranean Sea. Plant Physiology 101: 285-296

Peloquin J, Swan C, Gruber N, Vogt M, Claustre H, Ras J, Uitz J, Barlow R, Behrenfeld M, Bidigare R, Dierssen H, Ditullio G, Fernandez E, Gallienne C, Gibb S, Goericke R, Harding L, Head E, Holligan PM, Hooker SB, Karl D, Landry M, Letelier R, Llewellyn CA, Lomas N, Lucas M, Mannino A, Marty J-C, Mitchell BG, Muller-Karger F, Nelson N, O'Brien C, Prezelin B, Repeta D, Smith Jr WO, Smythe-Wright D, Stumpf R, Sybramaniam A, Suzuki K, Trees C, Vernet M, Wasmund N, Wright S (2013) The MAREDAT global database of high performance liquid chromatography marine pigment measurements. Earth System Science Data 5: 109-123

Perez V, Fernandez E, Maranon E, Moran XAG, Zubkovc MV (2006) Vertical distribution of phytoplankton biomass, production and growth in the Atlantic subtropical gyres. Deep-Sea Research, Part I 53: 1616-1634

Pham Thi NN, Huisman J, Sommeijer BP (2005) Simulation of three-dimensional phytoplankton dynamics: competition in light-limited environments. Journal of Computational and Applied Mathematics 174: 57-77

Polovina JJ, Howell EA, Abecassis M (2008) Ocean's least productive waters are expanding. Geophysical Research Letters 35: L03618. doi: 10.1029/2007GL031745

R Development Core Team (2012) R: A language and environment for statistical computing. http://www.R-project.org

Raven JA (1986) Physiological consequences of extremely small size for autotrophic organisms in the sea. In: Platt T, Li WKW (eds) Photosynthetic Picoplankton. Canadian Bulletin of Fisheries and Aquatic Sciences

Richardson AJ, Schoeman DS (2004) Climate impact on plankton ecosystems in the Northeast Atlantic. Science 305: 1609-1612

Ryabov AB, Rudolf L, Blasius B (2010) Vertical distribution and composition of phytoplankton under the influence of an upper mixed layer. Journal of Theoretical Biology 263: 120-133

Sarmiento JL (2004) Response of ocean ecosystems to climate warming. Global Biogeochemical Cycles 18: GB3003. doi: 10.1029/2003GB002134

Sarmiento JL, Hughes TMC, Stouffer RJ, Manabe S (1998) Simulated response of the ocean carbon cycle to anthropogenic climate warming. Nature 393: 245-249

Schoemann V, Becquevort S, Stefels J, Rousseau V, Lancelot C (2005) *Phaeocystis* blooms in the global ocean and their control mechanisms: a review. Journal of Sea Research 53: 43-66

Siegel DA, Doney SC, Yoder JA (2002) The North Atlantic spring phytoplankton bloom and Sverdrup's critical depth hypothesis. Science 296: 730-733

Stevens C, Smith M, Ross A (1999) SCAMP: measuring turbulence in estuaries, lakes, and coastal waters. NIWA - Water Atmosphere 7: 20-21

Sverdrup, E. U. 1953. On conditions for the vernal blooming of phytoplankton. Journal du Conseil / Conseil Permanent International pour l'Exploration de la Mer 18: 287-295

Talley L, Pickard G, Emery W, Swift J (2011) Typical distribution of water characteristics. Descriptive Physical Oceanography. Elsevier Ltd

Tarran GA, Heywood JL, Zubkov MV (2006) Latitudinal changes in the standing stocks of nano- and picoeukaryotic phytoplankton in the Atlantic Ocean. Deep-Sea Research, Part II 53: 1516-1529

Tungaraza C, Rousseau V, Brion V, Lancelot C, Gichuki J, Baeyens W, Goeyens L (2003) Contrasting nitrogen uptake by diatom and *Phaeocystis*-dominated phytoplankton assemblages in the North Sea. Journal of Experimental Marine Biology and Ecology 292: 19-41.

Uitz J, Claustre H, Morel A, Hooker SB (2006) Vertical distribution of phytoplankton communities in open ocean: An assessment based on surface chlorophyll. Journal of Geophysical Research 111: C08005. doi: 10.1029/2005JC003207

Uitz J, Huot Y, Bruyant F, Babin M, Claustre H (2008) Relating phytoplankton photophysiological properties to community structure on large scales. Limnology and Oceanography 53: 614-630

Unrein F, Gasol JM, Not F, Forn I, Massana R (2014) Mixotrophic haptophytes are key bacterial grazers in oligotrophic coastal waters. The ISME Journal 8: 164-176

van Aken HM (2000) The hydrography of the mid-latitude Northeast Atlantic Ocean II: The intermediate water masses. Deep-Sea Research, Part I 47: 789-824

van de Poll WH, Kulk G, Timmermans KR, Brussaard CPD, van der Woerd HJ, Kehoe MJ. Mojica KDA, Visser RJW, Rozeman PD, Buma AGJ (2013) Phytoplankton chlorophyll *a* biomass, composition, and productivity along a temperature and stratification gradient in the northeast Atlantic Ocean. Biogeosciences 10: 4227-4240

van de Waal DB, Verschoor AM, Verspagen JMH, Van Donk E, Huisman J (2010) Climate-driven changes in the ecological stoichiometry of aquatic ecosystems. Frontiers in Ecology and the Environment 8: 145-152

Vaulot D (1989) CYTOPC: Processing software for flow cytometric data. Signal and Noise 2: 8

Ward BA, Dutkiewicz S, Jahn O, Follows MJ (2012) A size-structured food-web model for the global ocean. Limnology and Oceanography 57: 1877-1891

Whitton BA, Potts M (eds) (2012) Ecology of cyanobacteria II: Their diversity in space and time. Springer Netherlands

Worden AZ, Nolan JK, Palenik B (2004) Assessing the dynamics and ecology of marine picophytoplankton: The importance of the eukaryotic component. Limnology and Oceanography 49: 168-179

Zinser ER, Johnson ZI, Coe A, Karaca E, Veneziano D, Chisholm SW (2007) Influence of light and temperature on *Prochlorococcus* ecotype distributions in the Atlantic Ocean. Limnology and Oceanography 52: 2205-2220

Zuur A, Ieno EN, Walker N, Saveliev AA, Smith GM (2009) Mixed Effects Models and Extensions in Ecology with R. Springer

Zuur AF, Ieno EN, Elphick CS (2010) A protocol for data exploration to avoid common statistical problems. Methods in Ecology and Evolution 1: 3-14